



1 **Atmospheric CO₂ estimates for the Miocene to Pleistocene based on foraminiferal $\delta^{11}\text{B}$**
2 **at Ocean Drilling Program Sites 806 and 807 in the Western Equatorial Pacific**

3
4 Maxence Guillermic^{1,2}, Sambuddha Misra^{3,4}, Robert Eagle^{1,2}, Aradhna Tripathi^{1,2}

5
6
7
8 ¹Department of Atmospheric and Oceanic Sciences, Department of Earth, Planetary, and
9 Space Sciences, Center for Diverse Leadership in Science, Institute of the Environment and
10 Sustainability, University of California – Los Angeles, Los Angeles, CA 90095 USA

11 ²Laboratoire Géosciences Océan UMR6538, UBO, Institut Universitaire Européen de la Mer,
12 Rue Dumont d'Urville, 29280, Plouzané, France

13 ³The Godwin Laboratory for Palaeoclimate Research, Department of Earth Sciences,
14 University of Cambridge, UK

15 ⁴Indian Institute of Science, Centre for Earth Sciences, Bengaluru, Karnataka 560012, India

16
17 *Correspondence to:* Maxence Guillermic (maxence.guillermic@gmail.com) and Aradhna
18 Tripathi (atripathi@g.ucla.edu)



19 **ABSTRACT**

20 Constraints on the evolution of atmospheric CO₂ levels throughout Earth's history are
21 foundational to our understanding of past variations in climate. Despite considerable effort,
22 estimates of past CO₂ levels do not always converge and therefore new records and proxies
23 are valuable. Here we reconstruct atmospheric CO₂ values across major climate transitions
24 over the past 17 million years using the boron isotopic composition ($\delta^{11}\text{B}$) of planktic
25 foraminifera from 89 samples obtained from two sites in the West Pacific Warm Pool, Ocean
26 Drilling Program (ODP) Sites 806 and 807. These sites are in a region that today is in
27 equilibrium with the atmosphere and are thought to have been in equilibrium with the
28 atmosphere for the interval studied. We use high-precision multi-collector inductively-
29 coupled plasma mass spectrometry and show that data from these sites can reproduce the ice
30 core record. Estimates of early Miocene pCO₂ are generally higher than published
31 reconstructions from other sites, while values for the Pliocene and Pleistocene are more
32 similar to other datasets. We find evidence for reductions in pCO₂ of ~280 μatm during the
33 Middle Miocene Climate Transition, ~270 μatm during Pliocene Glacial Intensification, and
34 ~50 μatm during the Mid-Pleistocene Climate Transition. There is possible evidence for a
35 larger reduction in glacial pCO₂ during the Mid-Pleistocene Transition compared to
36 interglacial pCO₂, and a minimum in pCO₂ during glacial MIS 30. Our results are consistent
37 with a coupling between pCO₂, temperature and ice sheet expansion throughout the past 17
38 million years.

39

40 **Highlights**

41 In this study, we are able to accurately reproduce pCO₂ data from ice cores using $\delta^{11}\text{B}$ data
42 from ODP Sites 806 and 807, demonstrating the fidelity of our approach. We therefore apply
43 the same framework to older samples to create a long-term pH and pCO₂ reconstruction for
44 the past 17 million years. We find major increases in surface water pH and decreases in
45 atmospheric pCO₂ were associated with decreased temperature in the Western Equatorial
46 Pacific, including associated with major episodes of ice sheet expansion in the high latitudes,
47 providing more robust quantitative constraints on the past coupling between pCO₂,
48 temperature, and cryosphere stability.

49

50 **Keywords**

51 Boron isotopes, CO₂, ODP Site 806, ODP Site 807, Miocene, climate



52 **1. Introduction**

53 Due to concerns about the long-term consequences of anthropogenic emissions and
54 associated climate change (IPCC, 2014, 2018), efforts have been made to quantify past
55 atmospheric CO₂ and examine past relationships between CO₂ and temperature. Such data are
56 not only critical for constraining Earth-system sensitivity (Lea, 2004; Lunt et al., 2010;
57 Pagani et al., 2010; Hansen et al., 2012, 2013, Foster and Rohling, 2013; Schmittner et al.,
58 2011; Tierney et al., 2020), but are also of broad interest because such data can help us
59 understand the evolution of climate and geological systems through Earth's history (Tripathi et
60 al., 2011; Foster et al., 2017; Tripathi and Darby, 2018). However, discrepancies between
61 proxy reconstructions still exist, including for major climate transitions of the Cenozoic. In
62 particular, there remains a pressing need for robust and higher-resolution atmospheric CO₂
63 records from sites that are in equilibrium with the atmosphere.

64 Relatively high-resolution and direct determinations of atmospheric CO₂ are available
65 for the last 800 kyr through analysis of air bubbles extracted from ice-cores, but these records
66 are limited to the availability of cores (Petit et al., 1999; Siegenthaler et al., 2005; Lüthi et al.,
67 2008). A window into atmospheric CO₂ levels comes from 1 million-year-old blue ice
68 (Higgins et al., 2015) and more recently from the Pliocene period (Yan et al., 2019). Most
69 reconstructions of CO₂ for prior to 800 ka are based on indirect terrestrial and marine proxies.
70 Stomata indices for fossil leaves (Van der Burgh, 1993; Royer, 2001), carbon isotope ratios
71 ($\delta^{13}\text{C}$) of paleosols (Retallak et al., 2009), $\delta^{13}\text{C}$ of alkenones (Pagani et al., 2005; Zhang et
72 al., 2013), B/Ca ratios of surface-dwelling foraminifera (Yu and Hönisch, 2007; Foster, 2008;
73 Tripathi et al., 2009, 2011), and boron isotope ratios ($\delta^{11}\text{B}$) of surface-dwelling foraminifera
74 (Pearson and Palmer, 2000; Hönisch et al., 2009; Bartoli et al., 2011; Foster et al., 2012;
75 Foster and Sexton, 2014; Chalk et al., 2017; Sosdian et al., 2018; Dyez et al., 2018) have
76 been used to estimate atmospheric CO₂.

77 Each of the above proxy methods has sources of systematic errors that we do not
78 attempt to exhaustively document as they have been discussed in-depth elsewhere (e.g.,
79 Pagani et al., 2005; Tripathi et al., 2011; Guillermic et al., 2020). However, we note that
80 significant developments in the boron-based proxies include improvements to the accuracy
81 and precision of measurements using multi-collector inductively coupled mass spectrometry
82 (MC-ICP-MS) compared to early work with thermal ionization mass spectrometry (TIMS),
83 where there were large instrumental mass fractionations and challenges with laboratory
84 intercomparison (Foster et al., 2013; Farmer et al., 2016; Aggarwal and You, 2017). There



85 was also the realization that temperature-dependent K_D to interpreting B/Ca sensitivities
86 observed from the field of sediment trap, core-top, and downcore studies (Yu and Hönisch,
87 2007; Foster et al., 2008; Tripathi et al., 2009, 2011; Babila et al., 2010; Osborne et al., 2020)
88 differ from foraminiferal culture experiments (Allen et al., 2011, 2012) and inorganic calcite
89 (Mavromatis et al., 2015); this type of discrepancy has also been observed with other
90 elemental proxies (e.g., Mg/Ca). Such differences may be due to differences in growth rates
91 (Sadekov et al., 2014), ontogenetic changes, a correlation in the field between temperature
92 and other hydrographic variables that obscure robust statistical determination of parameter
93 relationships, culture conditions resulting in organisms being stressed, and/or other factors.

94 The marine CO_2 proxy that appears to be subject to the fewest systematic
95 uncertainties, based on our current understanding, is the boron isotopic composition ($\delta^{11}\text{B}$) of
96 planktic foraminifera as measured using MC-ICPMS and TE-NTIMS. This proxy provides
97 constraints on seawater pH, if temperature, salinity, seawater $\delta^{11}\text{B}$, and the appropriate mono-
98 specific calibration between $\delta^{11}\text{B}_{\text{carbonate}}$ and $\delta^{11}\text{B}_{\text{borate}}$ are constrained (Pearson and Palmer,
99 2000; Foster et al., 2008; Sosdian et al., 2018; Raitzsch et al., 2018; Guillermic et al., 2020).
100 Seawater pH can be used to calculate seawater $p\text{CO}_2$ if there are constraints on a second
101 parameter of the carbonate system (e.g. alkalinity, DIC). Atmospheric $p\text{CO}_2$ can then be
102 constrained if the site being examined is in air-sea CO_2 equilibrium.

103 Given the evolution of the field, the number of studies generating high-precision and
104 high-resolution boron-based records over major climate transitions in the Cenozoic using the
105 recent analytical methods, and incorporating our current understanding of proxy systematics
106 are relatively few (Foster et al., 2012; Martinez-Boti et al., 2015b; Chalk et al., 2017, de la
107 Vega et al., 2020). Furthermore, of the existing studies using boron-based proxies, an
108 additional uncertainty frequently exists, namely the short time interval of study (e.g.,
109 emphasizing on a climate transition) (Martinez-Boti et al., 2015b; Chalk et al., 2017) and
110 whether the study sites remain in air-sea CO_2 equilibrium with the atmosphere (Martinez et
111 al., 2015a). And although estimation of atmospheric $p\text{CO}_2$ from seawater pH using this proxy
112 is relatively straightforward, reconstructions are still impacted by uncertainties including the
113 lack of robust constraints on a second parameter of the carbonate system, and our limited
114 understanding of secular variations in the $\delta^{11}\text{B}$ of seawater (Tripathi et al., 2011; Sosdian et al.,
115 2018; Greenop et al., 2017).

116 Therefore, to provide additional constraints on the evolution of atmospheric $p\text{CO}_2$
117 from the Miocene through Pleistocene, we developed new records from the western tropical



118 Pacific. We use foraminiferal $\delta^{11}\text{B}$ and trace elements in the planktic foraminiferal species
119 *Trilobus sacculifer* and *Globigerinoides ruber* to reconstruct past seawater pH and
120 atmospheric CO_2 at Ocean Drilling Program (ODP) Sites 806 and 807 in the Western
121 Equatorial Pacific (WEP) over the last 17 million years (Myr). The two sites we examined are
122 located on the western border of the tropical Pacific Ocean, the largest open-oceanic region
123 on the globe, and the warmest open ocean region at present. The west Pacific warm pool is a
124 region that is in air-sea CO_2 equilibrium (Takahashi et al., 2014), and is thought to have been
125 so throughout the Cenozoic so has been targeted for past atmospheric CO_2 reconstructions
126 (Pearson and Palmer, 2000; Tripathi et al., 2009, 2014).

127 This work represents the first reconstructions of past seawater pH and pCO_2 for the
128 WEP using MC-ICPMS, thereby providing an invaluable new perspective on reconstructing
129 past atmospheric CO_2 via marine sediment archives. We explore various constraints on the
130 second carbonate system parameter using a number of different scenarios, following on the
131 systematic work done by Tripathi et al. (2009) and (2011) for B/Ca. We interpret these data
132 using recent constraints on seawater $\delta^{11}\text{B}$ (Lemarchand et al., 2000; Raitzsch and Hönisch,
133 2013; Greenop et al., 2017). For temperature estimation, we utilize a multi-variable model for
134 Mg/Ca (Gray and Evans, 2019), that builds on prior work with clumped isotopes in planktic
135 foraminifera for Site 806 and other WEP sites demonstrating that for the Last Glacial
136 Maximum to recent, salinity-corrected Mg/Ca values are needed to yield convergent
137 estimates of mixed-layer temperatures (Tripathi et al., 2014).

138

139 **2. Materials and Methods**

140 Below we describe site locations, analytical methods used, and figures of merit. The
141 supplemental methods section describes screening for potential contamination, equations
142 used for calculations, and error propagation.

143

144 **2.1 Site locations**

145 Samples are from three ODP holes recovered during ODP Leg 130 in the WEP (Fig.
146 1, Table 1): ODP 806A ($0^\circ 19.140'\text{N}$, $159^\circ 21.660'\text{E}$, 2520.7 m water depth), ODP 806B
147 ($0^\circ 19.110'\text{N}$, $159^\circ 21.660'\text{E}$, 2519.9 m water depth), and ODP 807A ($3^\circ 36.420'\text{N}$,
148 $156^\circ 37.500'\text{E}$, 2803.8 m water depth) (Berger et al., 1993). Sites 806 and 807 are not likely to
149 have experienced major tectonic changes over the last 20 million years.



150 The WEP sites used in this study are in equilibrium with the atmosphere today
151 (Takahashi et al., 2014), and given their location, are thought to have been throughout the
152 Cenozoic (Pearson and Palmer, 2000; Tripathi et al., 2009, 2014). We do note, however, that
153 the thermocline is deep today, and that changes in thermocline depth have been inferred for
154 the WEP (Nathan and Leckie, 2009; Ford et al., 2015). Any potential changes in depth and
155 properties coupled with changes in upwelling, have the potential to influence equilibrium at
156 this site. While this is the case, changes should be smaller in the WEP compared to other
157 regions, due to the relatively small amplitude of changes in temperature and salinity (e.g.,
158 compared to eastern boundary current regions or higher latitude sites).

159

160 **2.2 Age models**

161 Sites 806 and 807 have high quality age models (Shackleton et al., 1991). The age
162 model for Site 806 from 0-1.35 Ma is based on Lea et al. (2000), while from 1.352-5.875 Ma
163 it is based on Lisiecki and Raymo, (2005), and Wara et al. (2005) is the source of information
164 for sediments older than 5.875 Ma. Ages for Site 807 are based on published biostratigraphy
165 (Berger et al., 1993) for 807 with additional constraints placed by Zhang et al., (2007) for the
166 interval from 0-0.550 Ma.

167

168 **2.3 Species and trace element cleaning**

169 Samples were picked and cleaned to remove clays at UCLA (Los Angeles, CA) and
170 the University of Western Brittany (Plouzane, France). 50-100 foraminifera shells were
171 picked from the 300-400 μ m fraction size for *T. sacculifer* (w/o sacc) and from the 250-300
172 μ m for *G. ruber* (white sensu stricto). Picked foraminifera were gently crushed, clays
173 removed, and checked for coarse-grained silicates. Samples were then cleaned using a full
174 reductive and oxidative cleaning protocol following Barker et al. (2003). A final leach step
175 with 0.001N HCl was done prior dissolution in 1N HCl. Boron purification used a published
176 microdistillation protocol (see Misra et al., 2014b, Guillermic et al., 2020 for more detailed
177 methods).

178

179 **2.4 Chemical purification and geochemical analysis**

180 Chemical separation was performed in a boron-free clean lab at the University of
181 Cambridge (Cambridge, UK). Calcium concentrations were measured on an ICP-AES
182 @Ultima 2 HORIBA at the Pôle Spectrometrie Océan (PSO), UMR6538 (Plouzané, France).



183 Elemental ratios (e.g. X/Ca ratios) were analyzed on a Thermo Scientific ®Element XR HR-
184 ICP-MS at the PSO, Ifremer (Plouzané, France). Boron isotopic measurements were carried
185 out on a Thermo Scientific ®Neptune+ MC-ICP-MS equipped with 10¹³ Ohm resistor
186 amplifiers (Lloyd et al., 2018) at the University of Cambridge (Cambridge, UK).

187

188 2.5 Standards

189 Variations in B isotope ratios are expressed in conventional delta (δ) notation with
190 δ¹¹B values reported against the reference standard NIST SRM 951 (NIST, Gaithersburg,
191 MD, USA):

$$192 \quad \delta^{11}\text{B} (\text{‰}) = 1000 \times \left(\frac{{}^{11}\text{B}/{}^{10}\text{B}_{\text{Sample}}}{{}^{11}\text{B}/{}^{10}\text{B}_{\text{NIST SRM 951}}} - 1 \right) \quad \text{eq. 1}$$

193 Multiple analyses of external standards were performed to ensure data quality. For
194 boron isotopic measurements, JC_P-1 (Geological Survey of Japan, Tsukuba, Japan, Gutjahr et
195 al., 2014) was used as a carbonate standard, and NEP, a *Porites sp* coral from University of
196 Western Australia and Australian National University was also used (McCulloch et al.,
197 2014). A boron isotope liquid standard, ERM[®] AE121 (certified δ¹¹B = 19.9 ± 0.6 ‰, SD),
198 was used to monitor reproducibility and drift during each session (Vogl and Rosner, 2012;
199 Foster et al., 2013; Misra et al., 2014b). For trace elements, external reproducibility was
200 determined using the consistency standard Cam-Wuellerstorfi (University of Cambridge)
201 (Misra et al., 2014b).

202

203 2.6 Figures of Merit

204 2.6.1 δ¹¹B analyses

205 Samples measured for boron isotopes typically ranged in concentration from 10 ppb B
206 (~5ng B) to 20 ppb B samples (~10ng B). Sensitivity was 10mV/ppb B (eg. 100mV for
207 10ppb B) in wet plasma at 50μl/min sample aspiration rate. The intensity of ¹¹B for a sample
208 at 10 ppb B was typically 104 ± 15 mV (2 SD, typical session) and closely matched the 98 ±
209 6 mV (2 SD, typical session) of the standard. Procedural boron blanks ranged from 15 pg B
210 to 65 pg B (contributed to less than <1% of the sample signal). The acid blank during
211 analyses was measured at ≤ 1mV on the ¹¹B (which also is < 1% of the sample intensity), and
212 no memory effect was seen within and across sessions.

213 External reproducibility was determined by analyzing the international standard JC_P-1
214 (Gutjahr et al., 2014) and a *Porites sp.* coral (NEP). The boron isotopic composition of JC_P-1



215 was measured at $24.06 \pm 0.20\%$ (2 SD, n=6) within error of published values of $24.37 \pm$
216 0.32% , $24.11 \pm 0.43\%$ and $24.42 \pm 0.28\%$ from Holcomb et al. (2015), Farmer et al. (2016)
217 and Sutton et al. (2018), respectively. Average values are $\delta^{11}\text{B}_{\text{NEP}} = 25.72 \pm 0.79\%$ (2 SD,
218 n=31) determined over 13 different analytical sessions, with each number representing a
219 separately processed sample from this study. These results are within error of published
220 values of $26.20 \pm 0.88\%$ (2 SD, n = 27) and $25.80 \pm 0.89\%$ (2 SD, n = 6), from Holcomb et
221 al. (2015) and Sutton et al. (2018), respectively. Data are reported in Supplementary Table B.
222

223 2.6.2 X/Ca analyses

224 Trace element (TE) analyses were conducted at a Ca concentration of either 10 or 30
225 ppm. Typical blanks for a 30 ppm Ca session were: ${}^7\text{Li} < 2\%$, ${}^{11}\text{B} < 7\%$, ${}^{25}\text{Mg} < 0.2\%$ and
226 ${}^{43}\text{Ca} < 0.02\%$. Additionally, blanks for a 10 ppm Ca session were: ${}^7\text{Li} < 2.5\%$, ${}^{11}\text{B} < 10\%$,
227 ${}^{25}\text{Mg} < 0.4\%$ and ${}^{43}\text{Ca} < 0.05\%$. Analytical uncertainty of a single measurement was
228 calculated from the reproducibility of the CamWuellestorf standard: $0.6 \mu\text{mol/mol}$ for Li/Ca,
229 $8 \mu\text{mol/mol}$ for B/Ca and 0.02 mmol/mol for Mg/Ca (2 SD, n=48). Data are reported in
230 Supplementary Table B.
231

232 2.7 Calculations

233 Figure 2 shows the planktic $\delta^{11}\text{B}$ and B/Ca data compared to other records (benthic
234 $\delta^{18}\text{O}$, planktic Mg/Ca, and shell weight), while Figures 3 and 4 show the different histories of
235 seawater $\delta^{11}\text{B}$ and alkalinity used for calculations, respectively. Details of calculations are in
236 the Supplemental methods. Following the approach of Tripathi et al. (2009, 2014), we
237 explored multiple scenarios for the evolution of seawater boron geochemistry (Fig. 3) and
238 alkalinity for calculations of $p\text{CO}_2$ (Fig. 4). During the interval overlapping with the ice core
239 record, we observe that the choice of model used does not make a significant difference in
240 reconstructed values (Fig. 5). During earlier time intervals, we see there is a greater
241 divergence, reflecting larger uncertainties in seawater $\delta^{11}\text{B}$ and alkalinity further back in
242 Earth history.

243 During the early Pliocene (~4.5 to 3.5 Ma) and prior to 10 Ma, calculations of $p\text{CO}_2$
244 diverge largely because of disagreement between studies estimating past seawater $\delta^{11}\text{B}$ (Fig.
245 5). However, we also found that reconstructed pH values that utilize each of the $\delta^{11}\text{B}_{\text{seawater}}$
246 histories are not significantly different, when the uncertainty in reconstructed pH is fully
247 propagated (Fig. 5 and 6; see also Hönisch et al., 2019). In contrast to the results from



248 Greenop et al. (2017), the record from Raitzsch and Hönisch, (2013) exhibits substantial
249 variations on shorter timescales. Such variability is a challenge to reconcile with the Li
250 isotope record of Misra and Froelich, (2012), given that Li has a shorter residence time than
251 boron while having similar sources and sinks. For the remainder of this study, we use the
252 $\delta^{11}\text{B}_{\text{seawater}}$ history from Greenop et al. (2017) because it is in good agreement with seawater
253 $\delta^7\text{Li}$ (Misra and Froelich, 2012).

254 The three alkalinity models used diverge prior to 9 Ma, with a maximum difference at
255 ~ 13 Ma that is also reflected in reconstructed pCO_2 (Fig. 6). However, all three models yield
256 pCO_2 estimates that are within error of each other when the full uncertainty is considered
257 (Fig. 6). For the remainder of the text, we utilize the model of Caves et al. (2016) for
258 alkalinity and the $\delta^{11}\text{B}_{\text{seawater}}$ determined by Greenop et al. (2017), as these represent the best
259 constrained estimates for these parameters at this time.

260

261 **3. Results and discussion**

262 **3.1 Reproducing pCO_2 from ice cores**

263 Validation of air-sea equilibrium in the WEP during the relatively large amplitude late
264 Pleistocene glacial/interglacial cycles was a primary goal for our work. In order to validate
265 our approach, we reconstructed pCO_2 for the last 800 kyr (Fig. 5). The two critical
266 diagnostics we use for method validation are: 1) that the reconstruction of pCO_2 is
267 representative of recent atmospheric CO_2 , and 2) that the boron-based reconstruction
268 empirically reproduces the record from ice cores. For the last 800 kyr, reconstructed pCO_2
269 values for Holes 806A and B and Site 807 are mostly within error of the records from the
270 Vostok and EPICA Dome C ice cores (Fig. 5, Petit et al., 1999, Siegenthaler et al., 2005,
271 Lüthi et al., 2008). Absolute values for the last glacial/interglacial cycle are also within error
272 of the ice cores values, with the exception of two data points at 47 and 79 ka that have lower
273 pCO_2 in comparison to ice core values. Between MIS 7 and 6, our reconstructions exhibit a
274 decrease in temperature (ΔT) of 2.4°C , an increase in pH (ΔpH) of 0.08 and a decrease in
275 pCO_2 (ΔpCO_2) of $58 \mu\text{atm}$. Between stage 3 and 1, we observed an increase of temperature
276 of 2.5°C , a decrease of pH of 0.13 and an increase in pCO_2 of $76 \mu\text{atm}$. These results
277 highlight that we are able to reproduce absolute measurements of atmospheric pCO_2 within
278 error of the ice core record, and reproduce the amplitude of changes between transitions, with
279 uncertainties typical for this type of work (Hönisch et al., 2019). We note that reconstructed
280 pCO_2 uncertainties could potentially be reduced using independent temperature proxies for



281 the WEP such as clumped isotope thermometry (Tripathi et al., 2010; 2014), a technique that is
282 not sensitive to the same sources of error as Mg/Ca thermometry, and therefore is an area
283 planned for future work.

284

285 3.2 Long-term record

286 Our reconstruction is consistent with published Mg/Ca estimates of early Pliocene to
287 recent temperatures at Site 806 (Medina-Elizalde et al., 2005, Wara et al., 2005; Tripathi et al.,
288 2009, 2011). Our reconstruction is also consistent with the work of Nathan and Leckie,
289 (2009) for time slices at ~7.3 and ~6.2 Ma, though we note that the SST in our study is
290 slightly higher (~2°C) than what was reported for the middle/late Miocene by Nathan and
291 Leckie, 2009 and Zhang et al., 2014, which could reflect the different methods used for
292 reconstructing temperature. Our temperature record over the last 17 Myr for the WEP (Fig.
293 6C) shows a gradual decrease between 17 and 6.5 Ma from $36.7^{\circ}\text{C} \pm 0.6^{\circ}\text{C}$ (2 SD, n=4) for
294 the Miocene Climate Optimum (MCO) to values of $28.8 \pm 3.4^{\circ}\text{C}$ (2 SD, n=67) over the last
295 6.5 Myr. From 6.5 Ma to present, we reconstruct a slight decrease in SSTs, with more
296 variability after the Mid-Pleistocene Transition (MPT). Raw $\delta^{11}\text{B}$ data (Fig. 2B) exhibit a
297 significant decrease (4.2‰) with increasing age for *T. sacculifer* from 16.5 Ma to present.
298 Reconstructed pH for the MCO are 7.80 ± 0.10 (SD, n=4), with an increase of ~0.27 to a
299 Holocene value of 8.18 ± 0.11 (n=2) (Fig. 6D).

300

301 3.3 Miocene

302 The study of Miocene climate is thought to provide a useful analog for changes
303 associated with global warming and melting of polar ice, in concert with ocean circulation
304 (Holbourn et al., 2013). The Miocene epoch (23-5.3 Ma) is characterized by a warm interval,
305 the Miocene Climate Optimum (~17-14 Ma - MCO), and an abrupt cooling during the
306 Middle Miocene Climate Transition (~15-13 Ma – MMCT) that led to the expansion of ice
307 on Antarctica and Greenland. Climate modeling supports a role for decreasing CO₂ in this
308 transition (DeConto and Pollard, 2003). However, proxies for CO₂ yield conflicting
309 reconstructions for the MCO and MMCT. Alkenone-based reconstructions do not show any
310 variations over the MCO and MMCT with pCO₂ below 300 ppm (Zhang et al., 2013).
311 However, it is a challenge to simulate the large-scale advance and retreat of Antarctic ice
312 with such low pCO₂ values (Gasson et al., 2016). In contrast, published $\delta^{11}\text{B}$ -based
313 reconstructions supports higher pCO₂ for the MCO of ~350-400 ppm (Foster et al., 2012),



314 300-500 ppm (Greenop et al., 2014) or ~470-630 ppm (Sosdian et al., 2018), although it is
315 unclear if these values accurately reflect the atmosphere given the sites may or may not have
316 been in equilibrium with the atmosphere.

317 Some of the highest $p\text{CO}_2$ values we reconstruct are during the MCO (Fig. 6E). For
318 the MCO, our estimates are $479 \pm 173 \mu\text{atm}$ (2 SD, $n=4$, Table 2). The middle Miocene
319 values we reconstruct are in line with previous studies (Greenop et al., 2014; Sosdian et al.,
320 2018). Sosdian et al. (2018) report values of 470 to 630 ppm depending on the model of
321 $\delta^{11}\text{B}_{\text{seawater}}$ chosen. We attribute the differences in $\delta^{11}\text{B}$ -based $p\text{CO}_2$ to the choice of
322 reconstruction methods and/or the different oceanographic settings at each site. All of the
323 boron isotope-based reconstructions do not support reconstructions from alkenones for the
324 Miocene (Pagani et al., 1999; 2005; Zhang et al., 2013). As thoughtfully discussed by Badger
325 et al. (2019), the response of CO_2 derived from alkenones is muted compared to boron-based
326 reconstructions of CO_2 , and this is possibly due to changes in coccolithophore calcification
327 based on recent studies (Bolton and Stoll, 2013; Bolton et al., 2016). During the MCO
328 relative maxima in $p\text{CO}_2$, our data support very warm sea surface temperatures in the WEP
329 ($36.7^\circ\text{C} \pm 0.6^\circ\text{C}$ 2SD, $n=4$; Fig. 7C and 8C), that merits further examination in future studies.
330 In fact, the highest temperatures recorded in our samples occur when there is a minimum in
331 the global composite record of $\delta^{18}\text{O}$ of benthic foraminifera (Zachos et al., 2001, 2008;
332 Tripathi and Darby, 2018).

333 During the MMCT, we find evidence for changes in $p\text{CO}_2$ and temperature in the
334 WEP (Fig. 7). From 13.5 to 12.9 Ma, we reconstruct an increase of pH ~ 0.24 and a major
335 decrease of $p\text{CO}_2$ of $\sim 243 \mu\text{atm}$ during an interval highlighted by Flower and Kennett,
336 (1996), who observed changes in $\delta^{18}\text{O}$ indicative of rapid East Antarctic Ice Sheet growth,
337 and enhanced organic carbon burial with a maximum $\delta^{13}\text{C}$ reached at ~ 13.6 Ma (Shevenell et
338 al., 2004; Holbourn et al., 2007). At the same time, we find evidence for a decline in SST of
339 3.4°C to a minimum of 33.3°C . The synchronous shifts in the $\delta^{13}\text{C}$ and $\delta^{18}\text{O}$ of benthic
340 foraminifera are consistent with increased carbon burial during colder periods, thus feeding
341 back into decreasing atmospheric CO_2 , and supporting the hypothesis that the drawdown of
342 atmospheric CO_2 can in part, be explained by enhanced export of organic carbon.

343

344 **3.4 Late Miocene**

345 The resolution of our data during the late Miocene is low, with a data gap from 12.5 to
346 9.2 Ma, and another gap between 6.5 and 5 Ma. We note the $p\text{CO}_2$ peak at ~ 9 Ma observed



347 by Sosdian et al. (2018) is not seen in our record although this is likely due to the low
348 resolution of our dataset. Between 8.8 and 6.5 Ma we find evidence for a decrease in
349 atmospheric CO₂ of 205 μatm associated with a decrease in temperature of 3.1 °C.

350

351 **3.5 CO₂ during Pliocene Warmth**

352 Oxygen isotope data from a global benthic foraminiferal stack show that the Pliocene
353 epoch (5.3-2.6 Ma) was initially characterized by warm conditions followed by the
354 intensification of glaciation that occurred in several steps, including during MIS M2 (3.312-
355 3.264 Ma), followed by the Middle Pliocene Warm Period (Lisiecki and Raymo, 2005).
356 Figure 5 shows that during the Early Pliocene warm interval, from 4.7 to 4.5 Ma, we
357 calculate high pCO₂ values of 541 ± 124 ppm (2 SD, n=3, Table 2).

358 The Middle Pliocene Warm Period (MPWP – 3.29-2.97 Ma) is considered a relevant
359 geological analogue for future climate change given ~3°C warmer global temperatures and
360 sea levels that were ~20 m higher than today (Dutton et al., 2015; Haywood et al., 2016), and
361 is a target for model intercomparison projects, for which accurate paleo-atmospheric pCO₂
362 estimates are critical (Haywood et al., 2016). Our data support values of 515 ± 119 μatm (2
363 SD, n = 4) are marginally consistent with previously published δ¹¹B-derived pCO₂ from ODP
364 Site 999 (Martinez-Boti et al., 2015b) but are higher than Bartoli et al. (2011), which was 320
365 ± 130 (2 SD, n=8) for Site 999, potentially due to instrument offset between N-TIMS and
366 MC-ICP-MS (Martinez-Boti et al., 2015b). Our values are higher in comparison to boron
367 isotope estimates from de La Vega et al. (2020) for Site 999 and calculations based on
368 Martinez-Boti et al., (2015b.) This can suggest differences in air-sea equilibrium between
369 sites. The pCO₂ trends in this study are similar to previous ones, the reconstructed pCO₂
370 show larger amplitude in our study. pCO₂ concentrations determined from ice cores from the
371 early Pleistocene have recently been published (Yan et al., 2019, Figs. 4 and 5), and those
372 values are in good agreement with our boron-derived pCO₂ at site 806/807 reported here, and
373 with previous boron-based studies (Hönisch et al., 2009; Stap et al., 2016; Chalk et al., 2017).

374

375 **3.6 Pliocene Glacial Intensification**

376 The warmth and local pCO₂ maxima of the MPWP was followed by a strong decrease
377 of temperature in upwelling and high latitude regions during from 3.3-2.7 Ma, coincident
378 with glacial intensification in the Northern Hemisphere. This climate transition was
379 hypothesized to be driven by the closure of the Panama seaway the opening of the high



380 latitudes and subsequent modifications of oceanic circulation (Haug and Tiedemann, 1998).
381 However, modeling from Lunt et al. (2008) supports an additional major role for CO₂ in the
382 glaciation. pCO₂ thresholds have been proposed to explain the intensification of Northern
383 Hemisphere Glaciation, with values proposed ranging from 280 μatm (DeConto et al., 2008)
384 to 200 to 400 μatm (Koenig et al., 2011).

385 From 3.3 to 3.0 Ma, our boron isotope-derived estimates of pCO₂ are typically 150
386 μatm higher than Bartoli et al. (2011), and de la Vega., (2020). This study, Martinez-Boti et
387 al. (2015b) and de la Vega et al., (2020) used an MC-ICP-MS so it is possible the differences
388 reflect changes in air-sea equilibrium recorded at Site 999 compared to Sites 806/807.

389 The reconstruction for the WEP exhibits multiple steps during the decline in pCO₂,
390 with a minimum observed at 4.42 Ma (360 (±¹¹⁷₈₅) μatm), at 3.45 Ma (323 (±¹⁰⁰₇₅) μatm) and at
391 2.67 Ma (269 (±⁷⁷₅₉) μatm) (Fig. 9). Those atmospheric CO₂ concentrations are consistent
392 with the pCO₂ thresholds proposed by both DeConto et al. (2008) and Koenig et al. (2011)
393 for the intensification of Northern Hemisphere glaciation and the low CO₂ (280 ppmv)
394 scenario from Lunt et al. (2008). We speculate that associated with Pliocene glacial
395 intensification, at 4.42, 3.45 and 2.67 Ma, it is possible that the declines in CO₂ and ice
396 growth in turn drove substantial changes in pole-to-equator temperature gradients and winds,
397 that in turn may have impacted iron cycling (Watson et al., 2000; Robinson et al., 2005;
398 Martinez-Garcia et al., 2011), stratification (Toggweiler, 1999; Sigman et al., 2010), and
399 other feedbacks that impact the amplitude of glacial/interglacial cycles and have been
400 implicated as factors that could have contributed to Pliocene glacial intensification.
401 Specifically, as the mean climate state of the planet became cooler, and glacial-interglacial
402 cycles became larger in amplitude, enhanced windiness and dust transport and upwelling
403 during glacials may have enhanced iron fertilization and subsequent carbon export. This
404 could explain why glacial/interglacial amplitudes in WEP pCO₂ values decrease from the
405 MPWP towards the Pleistocene, whereas variations in δ¹⁸O are increasing.

406

407 3.7 Pleistocene

408 During the Pleistocene (2.58-0.01 Ma), the climate system experienced a transition in
409 glacial/interglacial (G/I) variability from low amplitude, higher frequency and obliquity-
410 dominated oscillations (i.e., ~ 41 kyr) of the late Pliocene to the high amplitude, lower
411 frequency and eccentricity-dominated cycles (i.e., ~100 kyr) of the last 800 kyr. This
412 transition is termed the Middle Pleistocene Transition (0.8-1.2 Ma – MPT). Questions have



413 been raised about the role of atmospheric CO₂ during this transition, including using boron-
414 based proxies (Hönisch et al., 2009; Tripathi et al., 2011; Chalk et al., 2017). Previous boron
415 isotope studies have suggested that a decline in atmospheric CO₂ did not occur during the
416 MPT (Hönisch et al., 2009; Chalk et al., 2017; Dyez et al., 2018).

417 Although our pCO₂ results for the MPT are broadly in the range of values reported by
418 Hönisch et al. (2009) and Chalk et al. (2017), we have higher data coverage for the middle
419 and later part of the transition (Fig. 9D). Taken alone, or when combined with the published
420 data from Chalk et al. (2017) (that is also based on MC-ICPMS), our results support a
421 reduction of both glacial and interglacial pCO₂ values. We also find evidence that during the
422 MPT, glacial pCO₂ declined rapidly from 189 (±30) μatm at MIS 36 (Chalk et al., 2017) to
423 reach a minimum of 164 (±⁴⁴₃₅) μatm during MIS 30, the pCO₂ concentrations are however
424 within error when uncertainty is fully propagated, and then remained relatively stable until the
425 end of the MPT whereas interglacial pCO₂ values decrease gradually to reach post-MPT
426 values.

427 In our record for the last 17 Myr, the lowest pCO₂ is recorded at MIS 30 during the
428 MPT, with values of 164 (±⁴⁴₃₅) μatm, which supports an atmospheric CO₂ threshold that leads
429 to ice sheet stability. During this transition, the pCO₂ threshold needed to build sufficiently
430 large ice sheets that were able to survive the critical orbital phase of rising obliquity to
431 ultimately switch to a 100 kyr world, was likely reached at MIS 30. The multiple feedbacks
432 resulting from stable ice sheets (iron fertilization/productivity/changes in albedo/ changes in
433 deep water formation) might have sustained larger mean global ice volumes over the
434 subsequent 800 kyr. An asymmetrical decrease between pCO₂ values during interglacials
435 relative to glacials, with glacials exhibiting the largest change across the MPT, would have
436 led to increased sequestration of carbon during glacials in the 100 kyr world, as discussed by
437 Chalk et al. (2017), with increased glacial dust input and iron fertilization.

438

439 **3.8 Changes in volcanic activity and silicate weathering, and long-term pCO₂**

440 On million-year timescales, atmospheric CO₂ is mainly controlled by volcanic activity
441 and silicate weathering. Over the last 17 Myr, two relative maxima in atmospheric pCO₂ are
442 observed in our record, one during the MCO (at 15.67 Ma) and a second around the late
443 Miocene/early Pliocene (beginning at 4.7 and 4.5 Ma) (Fig. 10), though the timing for the
444 latter is not precise. The high CO₂ levels of the MCO are hypothesized (Foster et al., 2012) to
445 coincide with increasing volcanic activity, associated with the eruption of the Columbia River



446 Flood Basalts (Hooper et al., 2002; Kasbohm and Schoene, 2018), with recent
447 geochronologic evidence published supporting higher eruption activity between 16.7 and 15.9
448 Ma (Kasbohm and Schoene, 2018). The second CO₂ peak could correspond to observed
449 global increased volcanism in the early/middle Pliocene (Kennett and Thunell, 1977;
450 Kroenke et al., 1993), and/or a change of silicate weathering regime. Strontium and lithium
451 isotopes (^{87/86}Sr and δ⁷Li) have been used as proxy for silicate weathering activity. Although
452 the strontium isotope record exhibits a monotonous increase, lithium isotope data (Misra and
453 Froelich, 2012) are more variable with a transition from a period of increase seawater δ⁷Li
454 (e.g. non-steady state weathering) to stable seawater δ⁷Li (e.g., steady state weathering)
455 beginning at roughly 6.8 Ma (Fig. 10).

456

457 **3.9 History of the WEP**

458 The patterns observed in our study are also in line with major changes in the
459 equatorial Pacific dynamic reported from other studies over these timescales (Figure 8). The
460 development of the warm pool and transient changes between La Madre (La-Nina-like) to El
461 Padre (El-Nino-like conditions) have been inferred from geological records (Nathan and
462 Leckie, 2009), including foraminiferal assemblage data and asymmetric carbonate
463 preservation between the west and the east equatorial Pacific (Chaisson and Ravelo, 2000;
464 Nathan and Leckie, 2009), and sea surface and sub-surface temperature proxies (Wara et al,
465 2005; Rickaby and Halloran, 2005; Seki et al., 2012; Ford et al., 2012, 2015; Drury et al.,
466 2018).

467 The increase in CO₂ in the late Miocene and early Pliocene in our record corresponds
468 to the timing of the biogenic bloom in the Eastern equatorial Pacific that has been linked to a
469 global biogenic bloom (Hermoyan and Owen, 2001). These blooms have been hypothesized
470 to arise from an increase in nutrients (Hermoyan and Owen, 2001) that arose due to higher
471 rates of weathering as well as change in oceanic circulation due to Indonesian and Central
472 American Seaways constrictions (Gupta and Thomas, 1999; Grant and Dickens, 2002
473 amongst many others). The change in silicate weathering regime inferred from the record of
474 δ⁷Li (Misra and Froelich, 2012) would also be consistent with this hypothesis.

475

476 **3.9 Outlook and Conclusions**

477 We developed a reconstruction of atmospheric pCO₂ based on δ¹¹B of planktic
478 foraminifera from ODP Sites 806 and 807 located in the Western Equatorial Pacific for the



479 past 17 million years. Our study represents the first long-term reconstruction for the Neogene
480 derived from boron isotopes from the Pacific Ocean. We build on past efforts to reconstruct
481 atmospheric $p\text{CO}_2$ using different proxies from this region, including from carbon isotopes in
482 marine organic matter (Rayno et al., 1996) and alkenones (Pagani et al., 2010), as well as
483 foraminiferal B/Ca ratios (Tripathi et al., 2009, 2011), all of which have been shown to have a
484 number of complexities and potential sources of systematic error (e.g., Tripathi et al., 2011). It
485 also builds on efforts using boron isotopes in other regions using MC-ICP-MS (Seki et al.,
486 2010; Foster et al., 2012, 2014; Greenop et al., 2014; Martinez-Boti et al., 2015b; Stap et al.,
487 2016; Chalk et al., 2017; Dyez et al., 2018; de la Vega et al., 2020), and our recent work
488 constraining fractionation factors and measuring small samples of foraminifera. Although the
489 record is not continuous, with variable resolution, it captures both long-term and short-term
490 variability associated with several key transitions and demonstrates the utility of these sites
491 for future higher resolution study.

492 As expected, these data generally reproduce the $p\text{CO}_2$ record from ice cores,
493 consistent with the sites being in equilibrium with the atmosphere. The MCO has higher
494 $p\text{CO}_2$ than reconstructions from other sites, with values estimated as $479 \pm 173 \mu\text{atm}$ (2 SD,
495 $n=4$), potentially linked to the eruption of the Columbia River Flood Basalts, with values
496 declining into the early Pliocene. Major drops in $p\text{CO}_2$ occurred at 12.9, 4.42, 3.45 and 2.71
497 Ma, including during Pliocene glacial intensification. We find support for a larger reduction
498 in glacial $p\text{CO}_2$ during the MPT compared to interglacial $p\text{CO}_2$, and a minimum in $p\text{CO}_2$
499 during glacial MIS 30. These findings support a role for CO_2 in the transition from a 41 kyr
500 to a 100 kyr world.

501 Higher-resolution boron isotope records from the WEP would allow for further
502 resolution of these changes. Additional constraints on temperature, such as from clumped
503 isotopes (Tripathi et al., 2010) in the WEP (Tripathi et al., 2014), could allow for uncertainties
504 in $p\text{CO}_2$ estimates from boron isotopes to be reduced and for new constraints on Earth system
505 climate sensitivity. Future constraints on the vertical structure of the tropical Pacific during
506 these transitions may also potentially be illuminating.

507

508 **Acknowledgments**

509 The authors wish to thank the Tripathi Lab, including Lea Bonnin and Alexandra Villa, for
510 assistance with picking samples; the IODP core repository for provision of samples; Mervyn
511 Greaves for technical support and use of laboratory space at the University of Cambridge;



512 Yoan Germain, Emmanuel Ponzevera, Céline Liorzou and Oanez Lebeau for technical
513 support and use of laboratory space at IUEM and Ifremer (Plouzané, France).

514

515 **Financial support**

516 This research is supported by DOE BES grant no. DE-FG02-13ER16402 to AKT, by the
517 International Research Chair Program that is funded by the French government (LabexMer
518 ANR-10-LABX-19-01) to AKT and RAE, and IAGC student research grant 2017.

519

520 **6. References**

- Aggarwal, S. K., & You, C. F.: A review on the determination of isotope ratios of boron with mass spectrometry. *Mass Spectrometry Reviews*, 36(4), 499-519, 2017.
- Allen, K. A. and Hönisch, B.: The planktic foraminiferal B/Ca proxy for seawater carbonate chemistry, A critical evaluation, *Earth Planet. Sci. Lett.*, 345–348, 203–211, 2012.
- Allen, K. A., Hönisch, B., Eggins, S. M., Yu, J., Spero, H. J., Elderfield, H.: Controls on boron incorporation in cultured tests of the planktic foraminifer *Orbulina universa*. *Earth and Planetary Science Letters*, 309(3-4), 291-301, 2011.
- Anagnostou, E., John, E. H., Edgar, K. M., Foster, G. L., Ridgwell, A., Inglis, G. N., D. Pancost, R., J. Lunt, D., Pearson, P. N.: Changing atmospheric CO₂ concentration was the primary driver of early Cenozoic climate. *Nature*, 533(7603), 380-384, 2016.
- Babila, T., Huang, K. F., Rosenthal, Y., Conte, M. H., & Lin, H. L. Development of B/Ca as a seawater pH proxy using sediment trap time series, abstract, 2010.
- Badger M. P. S., Chalk T. B., Foster G. L., Bown P. R., Gibbs S. J., Sexton P. F., Schmidt D. N., Pälike H., Mackensen A. and Pancost R. D.: Insensitivity of alkenone carbon isotopes to atmospheric CO₂ at low to moderate CO₂ levels. *Climate of the Past*, 15(2), 539-554, 2019.
- Badger M. P. S., Lear C. H., Pancost R. D., Foster G. L., Bailey T. R., Leng M. J. and Abels H. A.: CO₂ drawdown following the middle Miocene expansion of the Antarctic Ice Sheet. *Paleoceanography* 28, 42–53, 2013.
- Barker S., Greaves M. and Elderfield H.: A study of cleaning procedures used for foraminiferal Mg/Ca paleothermometry. *Geochemistry, Geophys. Geosystems* 4, 1–20, 2003.
- Bartoli G., Hönisch B. and Zeebe R. E.: Atmospheric CO₂ decline during the Pliocene intensification of Northern Hemisphere glaciations. *Paleoceanography* 26, 1–14, 2011.
- Berger, W.H., Kroenke, J.W., Mayer, L.A.: *Proceedings of the Ocean Drilling Program, Scientific Results, Vol. 130*, 1993.
- Berger, W.H., Kroenke, L., Janecek, T.R., et al., . *Proceedings of the Ocean Drilling Program. Initial Reports*, p. 130, 1991.
- Bian, N., & Martin, P. A.: Investigating the fidelity of Mg/Ca and other elemental data from reductively cleaned planktonic foraminifera. *Paleoceanography*, 25(2), 2010.
- Bolton C. T. and Stoll H. M.: Late Miocene threshold response of marine algae to carbon dioxide limitation. *Nature* 500, 558–562, 2013.
- Bolton C. T., Hernández-Sánchez M. T., Fuertes M.-Á., González-Lemos S., Abrevaya L., Méndez-Vicente A., Flores J.-A., Probert I., Giosan L., Johnson J. and Stoll H. M. : Decrease in coccolithophore calcification and CO₂ since the middle Miocene. *Nat. Commun.* 7, 10284, 2016.



- Boyer, T.P., J. I. Antonov, O. K. Baranova, C. Coleman, H. E. Garcia, A. Grodsky, D. R. Johnson, R. A. Locarnini, A. V. Mishonov, T.D. O'Brien, C.R. Paver, J.R. Reagan, D. Seidov, I. V. Smolyar, and M. M. Zweng, 2013: World Ocean Database 2013, NOAA Atlas NESDIS 72, S. Levitus, Ed., A. Mishonov, Technical Ed.; Silver Spring, MD, 209 pp., <http://doi.org/10.7289/V5NZ85MT>, 2013.
- Brennan, S. T., Lowenstein, T. K., & Cendón, D. I. : The major-ion composition of Cenozoic seawater: The past 36 million years from fluid inclusions in marine halite. *American Journal of Science*, 313(8), 713-775, 2013.
- Caves J. K., Jost A. B., Lau K. V. and Maher K.: Cenozoic carbon cycle imbalances and a variable weathering feedback. *Earth Planet. Sci. Lett.* 450, 152–163, 2016.
- Chalk T. B., Hain M. P., Foster G. L., Rohling E. J., Sexton P. F., Badger M. P. S., Cherry S. G., Hasenfratz A. P., Haug G. H., Jaccard S. L., Martínez-García A., Pälike H., Pancost R. D. and Wilson P. A.: Causes of ice age intensification across the Mid-Pleistocene Transition. *Proc. Natl. Acad. Sci.*, 201702143, 2017.
- Coggon R. M., Teagle D. A. H. and Dunkley Jones T. Comment on “What do we know about the evolution of Mg to Ca ratios in seawater?” by Wally Broecker and Jimin Yu. *Paleoceanography* 26, 2011.
- DeConto, R. M., & Pollard, D.: Rapid Cenozoic glaciation of Antarctica induced by declining atmospheric CO₂. *Nature*, 421(6920), 245-249, 2003.
- DeConto R. M., Pollard D., Wilson P. A., Pälike H., Lear C. H. and Pagani M.: Thresholds for Cenozoic bipolar glaciation. *Nature* 455, 652–656, 2008.
- DeFantle M. S. and DePaolo D. J.: Sr isotopes and pore fluid chemistry in carbonate sediment of the Ontong Java Plateau: Calcite recrystallization rates and evidence for a rapid rise in seawater Mg over the last 10 million years. *Geochim. Cosmochim. Acta* 70, 3883–3904, 2006.
- Dekens P. S., Lea D. W., Pak D. K. and Spero H. J.: Core top calibration of Mg/Ca in tropical foraminifera: Refining paleotemperature estimation. *Geochemistry, Geophys. Geosystems* 3, 1–29, 2002.
- Delaney, M. L., Bé, A. W., & Boyle, E. A.: Li, Sr, Mg, and Na in foraminiferal calcite shells from laboratory culture, sediment traps, and sediment cores. *Geochimica et Cosmochimica Acta*, 49(6), 1327-1341, 1985.
- de la Vega, E., Chalk, T. B., Wilson, P. A., Bysani, R. P., & Foster, G. L.: Atmospheric CO₂ during the Mid-Piacenzian Warm Period and the M2 glaciation. *Scientific Reports*, 10(1), 1-8, 2020.
- Dickson A. G.: Thermodynamics of the Dissociation of Boric Acid in Potassium Chloride Solutions from 273.15 to 318.15 K. *J. Chem. Eng. Data* 35, 253–257, 1990.
- Drury, A. J., Lee, G. P., Gray, W. R., Lyle, M., Westerhold, T., Shevenell, A. E., & John, C. M.: Deciphering the state of the late Miocene to early Pliocene equatorial Pacific. *Paleoceanography and paleoclimatology*, 33(3), 246-263, 2018.
- Dyez, K. A., Hönisch, B., & Schmidt, G. A.: Early Pleistocene obliquity-scale pCO₂ variability at ~ 1.5 million years ago. *Paleoceanography and Paleoclimatology*, 33(11), 1270-1291, 2018.
- Evans, D. & Müller, W.: Deep time foraminifera Mg/Ca paleothermometry: Nonlinear correction for secular change in seawater Mg/Ca. *Paleoceanography* 27, PA4205, 2012.
- Evans, D., Wade, B. S., Henenhan, M., Erez, J., & Müller, W.: Revisiting carbonate chemistry controls on planktic foraminifera Mg/Ca: implications for sea surface temperature and hydrology shifts over the Paleocene–Eocene Thermal Maximum and Eocene–Oligocene transition. *Climate of the Past*, 12(4), 819-835, 2016.



- Farmer, J. R., Hönisch, B., & Uchikawa, J.: Single laboratory comparison of MC-ICP-MS and N-TIMS boron isotope analyses in marine carbonates. *Chemical Geology*, 447, 173–182, 2016.
- Farrell, J. W., Raffi, I., Janecek, T., Murray, D. W., Levitan, M., Dadey, K. A., Emeis, K. C., Lyle, M., Flores, J. A., Hovan, S.: Late Neogene sedimentation patterns in the eastern Equatorial Pacific Ocean. In: Pisias, N. G., Mayer, L. A., Janecek, T. R., Palmer-Julson, A., van Andel, T. H. (Eds.), *Proceedings of the Ocean Drilling Program. Scientific Results*, vol. 138. Ocean Drilling Program, College Station, TX, pp. 717–756, 1995.
- Flower, B. P., & Kennett, J. P.: Middle Miocene deepwater paleoceanography in the southwest Pacific: relations with East Antarctic Ice Sheet development. *Oceanographic Literature Review*, 8(43), 796, 1996.
- Ford, H. L., Ravelo, A. C., Dekens, P. S., LaRiviere, J. P., & Wara, M. W.: The evolution of the equatorial thermocline and the early Pliocene El Padre mean state. *Geophysical Research Letters*, 42(12), 4878–4887, 2015.
- Foster G. L.: Seawater pH, pCO₂ and [CO₂-3] variations in the Caribbean Sea over the last 130 kyr: A boron isotope and B/Ca study of planktic foraminifera. *Earth Planet. Sci. Lett.* 271, 254–266, 2008.
- Foster G. L. and Rohling E. J.: Relationship between sea level and climate forcing by CO₂ on geological timescales. *Proc. Natl. Acad. Sci.* 110, 1209–1214, 2013.
- Foster G. L. and Sexton P. F.: Enhanced carbon dioxide outgassing from the eastern equatorial Atlantic during the last glacial. *Geology* 42, 1003–1006, 2014.
- Foster, G. L., Hönisch, B., Paris, G., Dwyer, G. S., Rae, J. W., Elliott, T., Gaillardet, J., Hemming, N. G., Louvat, P., Vengosh, A.: Interlaboratory comparison of boron isotope analyses of boric acid, seawater and marine CaCO₃ by MC-ICPMS and NTIMS. *Chemical Geology*, 358, 1–14, 2013.
- Foster G. L., Lear C. H. and Rae J. W. B.: The evolution of pCO₂, ice volume and climate during the middle Miocene. *Earth Planet. Sci. Lett.* 341–344, 243–254, 2012.
- Foster G. L., Royer D. L. and Lunt D. J.: Future climate forcing potentially without precedent in the last 420 million years. *Nat. Commun.* 8, 14845. <http://dx.doi.org/10.1038/ncomms14845>, 2017.
- Gasson E., DeConto R. M., Pollard D. and Levy R. H.: Dynamic Antarctic ice sheet during the early to mid-Miocene. *Proc. Natl. Acad. Sci.* 113, 3459–3464, 2016.
- Gothmann A. M., Stolarski J., Adkins J. F., Schoene B., Dennis K. J., Schrag D. P., Mazur M. and Bender M. L.: Fossil corals as an archive of secular variations in seawater chemistry since the Mesozoic. *Geochim. Cosmochim. Acta* 160, 188–208, 2015.
- GraphPad Prism version 7.00 for Windows, GraphPad Software, La Jolla California USA, www.graphpad.com
- Gray, W. R., & Evans, D.: Nonthermal influences on Mg/Ca in planktonic foraminifera: a review of culture studies and application to the Last Glacial Maximum. *Paleoceanography and Paleoclimatology*, 34(3), 306–315, 2019.
- Gray, W. R., Weldeab, S., Lea, D. W., Rosenthal, Y., Gruber, N., Donner, B., & Fischer, G.: The effects of temperature, salinity, and the carbonate system on Mg/Ca in *Globigerinoides ruber* (white): A global sediment trap calibration. *Earth and Planetary Science Letters*, 482, 607–620, 2018.
- Greenop R., Foster G. L., Wilson P. A. and Lear C. H.: Middle Miocene climate instability associated with high-amplitude CO₂ variability. *Paleoceanography* 29, 845–853, 2014.
- Greenop R., Hain M. P., Sosdian S. M., Oliver K. I. C., Goodwin P., Chalk T. B., Lear C. H., Wilson P. A. and Foster G. L.: A record of Neogene seawater δ¹¹B reconstructed from



- paired $\delta^{11}\text{B}$ analyses on benthic and planktic foraminifera. *Clim. Past* 13, 149–170, 2017.
- Guillermic, M., Misra, S., Eagle, R., Villa, A., Chang, F., Tripathi, A.: Seawater pH reconstruction using boron isotopes in multiple planktonic foraminifera species with different depth habitats and their potential to constrain pH and pCO_2 gradients. *Biogeosciences*, 17(13), 3487–3510, 2020.
- Gutjahr, M., Bordier, L., Douville, E., Farmer, J., Foster, G. L., Hathorne, E., Hönisch, B., Lemarchand, D., Louvat, P., McCulloch, M., Noireaux, J., Pallavicini, N., Rodushkin, I., Roux, P., Stewart, J., Thil, F. You, C.F., Boron Isotope Intercomparison Project (BIIP): Development of a new carbonate standard for stable isotopic analyses. In EGU general assembly conference abstracts, Vol. 16, 2014.
- Hansen, J., Sato, M., & Ruedy, R.: Perception of climate change. *Proceedings of the National Academy of Sciences*, 109(37), 2012.
- Hansen J., Sato M., Russell G. and Kharecha P.: Climate sensitivity, sea level and atmospheric carbon dioxide. *Philos. Trans. R. Soc. A Math. Phys. Eng. Sci.* 371, 1–38, 2013.
- Haug, G. H., & Tiedemann, R.: Effect of the formation of the Isthmus of Panama on Atlantic Ocean thermohaline circulation. *Nature*, 393(6686), 673–676, 1998.
- Haywood, A. M., Dowsett, H. J., & Dolan, A. M.: Integrating geological archives and climate models for the mid-Pliocene warm period. *Nature communications*, 7(1), 1–14, 2016.
- Hemming N. G. and Hanson G. N.: Boron isotopic composition and concentration in modern marine carbonates. *Geochim. Cosmochim. Acta* 56, 537–543, 1992.
- Henehan M. J., Foster G. L., Bostock H. C., Greenop R., Marshall B. J. and Wilson P. A.: A new boron isotope-pH calibration for *Orbulina universa*, with implications for understanding and accounting for ‘vital effects.’ *Earth Planet. Sci. Lett.* 454, 282–292, 2016.
- Henehan M. J., Rae J. W. B., Foster G. L., Erez J., Prentice K. C., Kucera M., Bostock H. C., Martínez-Botí M. A., Milton J. A., Wilson P. A., Marshall B. J. and Elliott T. (2013) Calibration of the boron isotope proxy in the planktonic foraminifera *Globigerinoides ruber* for use in palaeo- CO_2 reconstruction. *Earth Planet. Sci. Lett.* 364, 111–122, 2013.
- Higgins J. A., Kurbatov A. V., Spaulding N. E., Brook E., Introne D. S., Chimiak L. M., Yan Y., Mayewski P. A. and Bender M. L.: Atmospheric composition 1 million years ago from blue ice in the Allan Hills, Antarctica. *Proc. Natl. Acad. Sci.* 112, 6887–6891, 2015.
- Holbourn A., Kuhnt W., Frank M. and Haley B. A.: Changes in Pacific Ocean circulation following the Miocene onset of permanent Antarctic ice cover. *Earth Planet. Sci. Lett.* 365, 38–50, 2013.
- Holcomb M., DeCarlo T. M., Schoepf V., Dissard D., Tanaka K. and McCulloch M.: Cleaning and pre-treatment procedures for biogenic and synthetic calcium carbonate powders for determination of elemental and boron isotopic compositions. *Chem. Geol.* 398, 11–21, 2015.
- Hönisch, B. and Hemming, N. G., Ground-truthing the boron isotope-paleo-pH proxy in planktonic foraminifera shells: Partial dissolution and shell size effects, *Paleoceanography* 19, 1–13, 2004.
- Hönisch, B., Allen, K. A., Lea, D. W., Spero, H. J., Eggins, S. M., Arbuszewski, J., deMenocal, P., Rosenthal, Y., D. Russel, a.: Elderfield, H.: The influence of salinity on Mg/Ca in planktic foraminifera—Evidence from cultures, core-top sediments and complementary $\delta^{18}\text{O}$. *Geochimica Et Cosmochimica Acta*, 121, 196–213, 2013.



- Hönisch, B., Eggins, S. M., Haynes, L. L., Allen, K. A., Holland, K. D., & Lorbacher, K.: Boron Proxies in Paleoceanography and Paleoclimatology. John Wiley & Sons, 2019.
- Hönisch B., Hemming N. G., Archer D., Siddall M. and McManus J. F.: Atmospheric carbon dioxide concentration across the mid-pleistocene transition. *Science* 324, 1551–1554, 2009.
- Horita J., Zimmermann H. and Holland H. D.: Chemical evolution of seawater during the Phanerozoic: Implications from the record of marine evaporites. *Geochim. Cosmochim. Acta* 66, 3733–3756., 2002.
- IPCC: Climate Change 2014 - The Physical Science Basis, edited by Intergovernmental Panel on Climate Change, Cambridge University Press, Cambridge., 2014.
- IPCC: Global Warming of 1.5 °C- edited by Intergovernmental Panel on Climate Change, 2018.
- Johnstone, H. J., Lee, W., & Schulz, M.: Effect of preservation state of planktonic foraminifera tests on the decrease in Mg/Ca due to reductive cleaning and on sample loss during cleaning. *Chemical Geology*, 420, 23-36, 2016.
- Kasbohm, J., & Schoene, B.: Rapid eruption of the Columbia River flood basalt and correlation with the mid-Miocene climate optimum. *Science advances*, 4(9), eaat8223, 2018.
- Kennett, J. P., & Thunell, R. C.: On explosive Cenozoic volcanism and climatic implications. *Science*, 196(4295), 1231-1234, 1977.
- Kısakürek, B., Eisenhauer, A., Böhm, F., Garbe-Schönberg, D., & Erez, J.: Controls on shell Mg/Ca and Sr/Ca in cultured planktonic foraminiferan, *Globigerinoides ruber* (white). *Earth and Planetary Science Letters*, 273(3-4), 260-269, 2008.
- Klochko K., Kaufman A. J., Yao W., Byrne R. H. and Tossell J. A.: Experimental measurement of boron isotope fractionation in seawater. *Earth Planet. Sci. Lett.* 248, 261–270, 2006.
- Koenig S. J., DeConto R. M. and Pollard D.: Late Pliocene to Pleistocene sensitivity of the Greenland Ice Sheet in response to external forcing and internal feedbacks. *Clim. Dyn.* 37, 1247–1268, 2011.
- Kroenke, L. W., Berger, W. H., Janecek, T. R. and Shipboard Scientific Party: Proceedings of the Ocean Drilling Program, Initial Reports, Vol. 130, 1991.
- Lea, D. W.: The 100 000-yr cycle in tropical SST, greenhouse forcing, and climate sensitivity. *Journal of Climate*, 17(11), 2170-2179, 2004.
- Lee, K., Kim, T. W., Byrne, R. H., Millero, F. J., Feely, R. A., & Liu, Y. M.: The universal ratio of boron to chlorinity for the North Pacific and North Atlantic oceans. *Geochimica et Cosmochimica Acta*, 74(6), 1801-1811, 2010.
- Lea, D. W., Pak, D. K., & Spero, H. J.: Climate impact of late Quaternary equatorial Pacific sea surface temperature variations. *Science*, 289(5485), 1719-1724, 2000.
- Lemarchand D., Gaillardet J., Lewin and Allégre C. J.: The influence of rivers on marine boron isotopes and implications for reconstructing past ocean pH. *Nature* 408, 951–954, 2000.
- Lisiecki L. E. and Raymo M. E.: A Pliocene-Pleistocene stack of 57 globally distributed benthic $\delta^{18}\text{O}$ records. *Paleoceanography* 20, 1–17, 2005.
- Lloyd, N. S., Sadekov, A. Y. and Misra, S., Application of 1013ohm Faraday cup current amplifiers for boron isotopic analyses by solution mode and laser ablation multicollector inductively coupled plasma mass spectrometry, *Rapid Commun. Mass Spectrom.*, 32, 9–18, 2018.
- Lueker, T. J., Dickson, A. G., & Keeling, C. D.: Ocean pCO₂ calculated from dissolved inorganic carbon, alkalinity, and equations for K₁ and K₂: validation based on



- laboratory measurements of CO₂ in gas and seawater at equilibrium. *Marine chemistry*, 70(1-3), 105-119, 2000.
- Lunt D. J., Foster G. L., Haywood A. M. and Stone E. J.: Late Pliocene Greenland glaciation controlled by a decline in atmospheric CO₂ levels. *Nature* 454, 1102–1105, 2008.
- Lunt, D. J., Haywood, A. M., Schmidt, G. A., Salzmann, U., Valdes, P. J., & Dowsett, H. J.: Earth system sensitivity inferred from Pliocene modelling and data. *Nature Geoscience*, 3(1), 60-64, 2010.
- Lüthi D., Le Floch M., Bereiter B., Blunier T., Barnola J. M., Siegenthaler U., Raynaud D., Jouzel J., Fischer H., Kawamura K. and Stocker T. F.: High-resolution carbon dioxide concentration record 650,000–800,000 years before present. *Nature* 453, 379–382, 2008.
- Martínez-Botí, M. A., Marino G., Foster G. L., Ziveri P., Henehan M. J., Rae J. W. B., Mortyn P. G. and Vance D.: Boron isotope evidence for oceanic carbon dioxide leakage during the last deglaciation. *Nature* 518, 219–222, 2015.
- Martínez-García, A., Rosell-Melé, A., Jaccard, S. L., Geibert, W., Sigman, D. M., & Haug, G. H.: Southern Ocean dust–climate coupling over the past four million years. *Nature*, 476(7360), 312-315, 2011.
- Mavromatis, V., Montouillout, V., Noireaux, J., Gaillardet, J. and Schott, J., Characterization of boron incorporation and speciation in calcite and aragonite from co-precipitation experiments under controlled pH, temperature and precipitation rate, *Geochim. Cosmochim. Acta*, 150, 299–313, 2015.
- McCulloch M. T., Holcomb M., Rankenburg K. and Trotter J. A.: Rapid, high-precision measurements of boron isotopic compositions in marine carbonates. *Rapid Commun. Mass Spectrom.* 28, 2704–2712, 2014.
- Medina-Elizalde M. and Lea D. W.: The mid-pleistocene transition in the tropical Pacific. *Science* 310, 1009–1012, 2005.
- Misra, S. and Froelich, P. N.: Lithium isotope history of Cenozoic seawater: Changes in silicate weathering and reverse weathering. *Science* (80-.). 335, 818–823, 2012.
- Misra, S., Greaves, M., Owen, R., Kerr, J., Elmore, A. C. and Elderfield, H.: Determination of B/Ca of natural carbonates by HR-ICP-MS. *Geochemistry, Geophys. Geosystems* 15, 1617–1628, 2014a.
- Misra, S., Owen, R., Kerr, J., Greaves, M. and Elderfield, H.: Determination of $\delta^{11}\text{B}$ by HR-ICP-MS from mass limited samples: Application to natural carbonates and water samples. *Geochim. Cosmochim. Acta* 140, 531–552, 2014b.
- Nathan, S. A., & Leckie, R. M.: *Palaeogeography, Palaeoclimatology, Palaeoecology*, 274(3-4), 140-159, 2009.
- Ni Y., Foster G. L., Bailey T., Elliott T., Schmidt D. N., Pearson P., Haley B. and Coath C.: A core top assessment of proxies for the ocean carbonate system in surface-dwelling foraminifers. *Paleoceanography* 22, 2007.
- Nir O., Vengosh A., Harkness J. S., Dwyer G. S. and Lahav O.: Direct measurement of the boron isotope fractionation factor: Reducing the uncertainty in reconstructing ocean paleo-pH. *Earth Planet. Sci. Lett.* 414, 1–5, 2015.
- Nürnberg, D., Bijma, J., & Hemleben, C.: Assessing the reliability of magnesium in foraminiferal calcite as a proxy for water mass temperatures. *Geochimica et Cosmochimica Acta*, 60(5), 803-814, 1996.
- O'Brien C. L., Foster G. L., Martínez-Botí M. A., Abell R., Rae J. W. B. and Pancost R. D.: High sea surface temperatures in tropical warm pools during the Pliocene. *Nat. Geosci.* 7, 606–611, 2014.
- Osborne, E. B., Umling, N. E., Bizimis, M., Buckley, W., Sadekov, A., Tappa, E., Marshall, B., R. Sautter, L., Thunell, R. C.: A Sediment Trap Evaluation of B/Ca as a Carbonate



- System Proxy in Asymbiotic and Nondinoflagellate Hosting Planktonic Foraminifera. *Paleoceanography and Paleoclimatology*, 35(2), 2020.
- Pagani P., Freeman G., Arthur F., Schuster M., Tiercelin J.-J. and Brunet M.: Late miocene atmospheric CO₂ concentrations and the expansion of C(4) grasses. *Science* 285, 876–9, 1999.
- Pagani M., Liu Z., Lariviere J. and Ravelo A. C.: High Earth-system climate sensitivity determined from Pliocene carbon dioxide concentrations. *Nat. Geosci.* 3, 27–30, 2010.
- Pagani M., Zachos J. C., Freeman K. H., Tipple B. and Bohaty S.: Atmospheric science: Marked decline in atmospheric carbon dioxide concentrations during the Paleogene. *Science* 309, 600–603, 2005.
- Pearson, P. N., & Palmer, M. R.: Atmospheric carbon dioxide concentrations over the past 60 million years. *Nature*, 406(6797), 695-699, 2000.
- Perez, F. F., & Fraga, F.: Association constant of fluoride and hydrogen ions in seawater. *Marine Chemistry*, 21(2), 161-168, 1987.
- Petit J. R., Jouzel J., Raynaud D., Barkov N. I., Barnola J. M., Basile I., Bender M., Chappellaz J., Davis M., Delaygue G., Delmotte M., Kotiyakov V. M., Legrand M., Lipenkov V. Y., Lorius C., Pépin L., Ritz C., Saltzman E. and Stievenard M.: Climate and atmospheric history of the past 420,000 years from the Vostok ice core, Antarctica. *Nature* 399, 429–436, 1999.
- Pierrot, D., Lewis, E., & Wallace, D. W. R.: MS Excel program developed for CO₂ system calculations. ORNL/CDIAC-105a. Carbon Dioxide Information Analysis Center, Oak Ridge National Laboratory, US Department of Energy, Oak Ridge, Tennessee, 10, 2006.
- Raitzsch M. and Hönisch B.: Cenozoic boron isotope variations in benthic foraminifers. *Geology* 41, 591–594, 2013.
- Raitzsch M., Bijma J., Benthien A., Richter K. U., Steinhofel G. and Kučera M.: Boron isotope-based seasonal paleo-pH reconstruction for the Southeast Atlantic – A multispecies approach using habitat preference of planktonic foraminifera. *Earth Planet. Sci. Lett.* 487, 138–150, 2018.
- Ravelo, A. C., Lawrence, K. T., Fedorov, A., & Ford, H. L.: Comment on “A 12-million-year temperature history of the tropical Pacific Ocean”. *Science*, 346(6216), 1467-1467, 2014.
- Retallack G. J.: Greenhouse crises of the past 300 million years. *Geol. Soc. Am. Bull.* 121, 1441–1455, 2009.
- Rickaby, R. E. M. and Halloran, P.: Cool La Nina During the Warmth of the Pliocene?, *Science*, 307, 1948–1952, 2005.
- Ridgwell A. and Zeebe R. E.: The role of the global carbonate cycle in the regulation and evolution of the Earth system. *Earth Planet. Sci. Lett.* 234, 299–315, 2005.
- Royer D. L.: Stomatal density and stomatal index as indicators of paleoatmospheric CO₂ concentration. *Rev. Palaeobot. Palynol.* 114, 1–28, 2001.
- Russell, A. D., Hönisch, B., Spero, H. J., & Lea, D. W.: Effects of seawater carbonate ion concentration and temperature on shell U, Mg, and Sr in cultured planktonic foraminifera. *Geochimica et Cosmochimica Acta*, 68(21), 4347-4361, 2004.
- Schmittner, A., Urban, N. M., Shakun, J. D., Mahowald, N. M., Clark, P. U., Bartlein, P. J., Mix A. C., Rosell-Melé, A.: Climate sensitivity estimated from temperature reconstructions of the Last Glacial Maximum. *Science*, 334(6061), 1385-1388, 2011.
- Seki O., Foster G. L., Schmidt D. N., Mackensen A., Kawamura K. and Pancost R. D.: Alkenone and boron-based Pliocene pCO₂ records. *Earth Planet. Sci. Lett.* 292, 201–211, 2010.



- Shackleton N.J., Berger A., Peltier W.R.: Trans. R. Soc. Edinb. Earth Sci. 81, 251.
Shipboard Leg, O. D. P., Map, O. D. P., & Map, D. S. D.: P. Initial Reports: Volume 130. doi:10.2973/odp.proc.ir.130.108.1991, 1991.
- Shevenell, A. E., Kennett, J. P., & Lea, D. W.: Middle Miocene southern ocean cooling and Antarctic cryosphere expansion. *Science*, 305(5691), 1766-1770, 2004.
- Schlitzer, R., Ocean Data View, <https://odv.awi.de>, 2016.
- Siegenthaler, U., Stocker, T. F., Monnin, E., Lüthi, D., Schwander, J., Stauffer, B., Raynaud, D., Barnola, J.M., Fischer, H., Masson-Delmotte, V., Jouzel, J.: Stable carbon cycle–climate relationship during the late Pleistocene. *Science*, 310(5752), 1313-1317, 2005.
- Sosdian, S. M., Greenop R., Hain M. P., Foster G. L., Pearson P. N. and Lear C. H.: Constraining the evolution of Neogene ocean carbonate chemistry using the boron isotope pH proxy. *Earth Planet. Sci. Lett.* 498, 362–376, 2018.
- Stap L. B., de Boer B., Ziegler M., Bintanja R., Lourens L. J. and van de Wal R. S. W.: CO₂ over the past 5 million years: Continuous simulation and new $\delta^{11}\text{B}$ -based proxy data. *Earth Planet. Sci. Lett.* 439, 1–10, 2016.
- Sutton J. N., Liu Y.-W., Ries J. B., Guilleminic M., Ponzevera E. and Eagle R. A.: $\delta^{11}\text{B}$ as monitor of calcification site pH in divergent marine calcifying organisms. *Biogeosciences* 15, 1447–1467, 2018.
- Takahashi T., Sutherland S. C., Chipman D. W., Goddard J. G. and Ho C.: Climatological distributions of pH, pCO₂, total CO₂, alkalinity, and CaCO₃ saturation in the global surface ocean, and temporal changes at selected locations. *Mar. Chem.* 164, 95–125, 2014.
- Tan, N., Ramstein, G., Dumas, C., Contoux, C., Ladant, J. B., Sepulchre, P., Zhang, Z., De Schepper, S.: Exploring the MIS M2 glaciation occurring during a warm and high atmospheric CO₂ Pliocene background climate. *Earth and Planetary Science Letters*, 472, 266-276, 2017.
- Tierney, J. E., Zhu, J., King, J., Malevich, S. B., Hakim, G. J., & Poulsen, C. J. (2020). Glacial cooling and climate sensitivity revisited. *Nature*, 584(7822), 569-573.
- Thomas, E.: Descent into the Icehouse. *Geology* 36, 191–192, 2008.
- Toggweiler, J. R.: Variation of atmospheric CO₂ by ventilation of the ocean's deepest water. *Paleoceanography*, 14(5), 571-588, 1999.
- Tripati, A., & Darby, D.: Evidence for ephemeral middle Eocene to early Oligocene Greenland glacial ice and pan-Arctic sea ice. *Nature communications*, 9(1), 1-11, 2018
- Tripati A. K., Roberts C. D. and Eagle R. A.: Coupling of CO₂ and Ice sheet stability over major climate transitions of the last 20 million years. *Science* (80-). 326, 1394–1397, 2009.
- Tripati A. K., Roberts C. D., Eagle R. A. and Li G.: A 20 million year record of planktic foraminiferal B/Ca ratios: Systematics and uncertainties in pCO₂ reconstructions. *Geochim. Cosmochim. Acta* 75, 2582–2610.
<http://dx.doi.org/10.1016/j.gca.2011.01.018>, 2011.
- Tyrrell, T., & Zeebe, R. E.: History of carbonate ion concentration over the last 100 million years. *Geochimica et Cosmochimica Acta*, 68(17), 3521-3530, 2004.
- Van Der Burgh J., Visscher H., Dilcher D. L. and Kürschner W. M.: Paleoatmospheric signatures in Neogene fossil leaves. *Science* 260, 1788–1790, 1993.
- Vogl J. and Rosner M.: Production and Certification of a Unique Set of Isotope and Delta Reference Materials for Boron Isotope Determination in Geochemical, Environmental and Industrial Materials. *Geostand. Geoanalytical Res.* 36, 161–175, 2012.
- Wara M. W., Ravelo A. C. and Delaney M. L.: Climate change: Permanent El Niño-like conditions during the Pliocene warm period. *Science* 309, 758–761, 2005.



- Yan, Y., Bender, M. L., Brook, E. J., Clifford, H. M., Kemeny, P. C., Kurbatov, A. V., Mackay, S., Mayewski, P.A., Ng, J., Severinghaus, J.P., Higgins, J. A.: Two-million-year-old snapshots of atmospheric gases from Antarctic ice. *Nature*, 574(7780), 663-666, 2019.
- Yu, J., Elderfield, H., Greaves, M., & Day, J.: Preferential dissolution of benthic foraminiferal calcite during laboratory reductive cleaning. *Geochemistry, Geophysics, Geosystems*, 8(6), 2007a.
- Yu J., Elderfield H. and Hönisch B.: B/Ca in planktonic foraminifera as a proxy for surface seawater pH. *Paleoceanography* 22, 2007.
- Zachos J. C., Dickens G. R. and Zeebe R. E.: An early Cenozoic perspective on greenhouse warming and carbon-cycle dynamics. *Nature* 451, 279–283, 2008.
- Zachos, J., Pagani, M., Sloan, L., Thomas, E., & Billups, K.: Trends, rhythms, and aberrations in global climate 65 Ma to present. *science*, 292(5517), 686-693, 2001.
- Zeebe R. E. and Wolf-Gladrow D.: CO₂ in Seawater: Equilibrium, Kinetics, Isotopes Elsevier Oceanography Series 65, Amsterdam, 2001.
- Zhang Y. G., Pagani M., Liu Z., Bohaty S. M. and Deconto R.: A 40-million-year history of atmospheric CO₂. *Philos. Trans. R. Soc. A Math. Phys. Eng. Sci.* 371, 20130096–20130096, 2013.
- Zhang, Y. G., Pagani, M., & Liu, Z.: A 12-million-year temperature history of the tropical Pacific Ocean. *Science*, 344(6179), 84-87, 2014.
- Zhang, J., Wang, P., Li, Q., Cheng, X., Jin, H., & Zhang, S.: Western equatorial Pacific productivity and carbonate dissolution over the last 550 kyr: Foraminiferal and nannofossil evidence from ODP Hole 807A. *Marine Micropaleontology*, 64(3-4), 121-140, 2007.



Figure captions

Figure 1: Modern hydrography of sites. **A.** Map of air-sea $p\text{CO}_2$ ($\Delta p\text{CO}_2$, μatm , data from Takahashi et al., 2014 and plotted using Ocean Data View from Schlitzer, 2016) showing the location of ODP Sites 806 and 807 (black circles). Depth profiles are for preindustrial parameters, **B.** pH calculated from GLODAP database and corrected from anthropogenic inputs, **C.** Boron isotopic composition of borate ion ($\delta^{11}\text{B}_{\text{borate}}$) with associated propagated uncertainties.

Figure 2: Foraminiferal data for the Miocene to Recent. **A.** Benthic foraminiferal $\delta^{18}\text{O}$ data (blue line – stack from Lisiecki and Raymo, 2005; black line – compilation from Zachos et al., 2008). **B.** $\delta^{11}\text{B}$ of *T. sacculifer* and *G. ruber* at Sites 806, 807. **C.** B/Ca ratios. **D.** Mg/Ca ratios. **E.** Calculated weight per shell for *T. sacculifer* and *G. ruber*. For Panels B-E: Circles = *T. sacculifer*, Triangles = *G. ruber*.

Figure 3: Different models for the evolution of the boron geochemistry explored as part of this work. Due to the 1‰ uncertainty propagated for $\delta^{11}\text{B}_{\text{seawater}}$, all scenarios yield reconstructed seawater pH values that are within error of each other. Propagated uncertainties were calculated using eq. S14 (see Supplement). **A.** Different models for $\delta^{11}\text{B}_{\text{seawater}}$ used for the reconstruction of $p\text{CO}_2$ in this study (blue – Lemarchand et al., 2000; green – Greenop et al., 2017; red – Raitzsch and Hönisch, 2013). **B.** Reconstructed pH based on our measured $\delta^{11}\text{B}_{\text{carbonate}}$ values using different models for $\delta^{11}\text{B}_{\text{seawater}}$.

Figure 4: Different models for the evolution of a second carbonate system parameter explored as part of this work. The propagated uncertainties were calculated using eq. S16 (see Supplement). **A.** Different models for alkalinity used for the reconstruction of $p\text{CO}_2$ in this study (orange - Ridgwell and Zeebe, 2005; violet - Tyrell and Zeebe, 2004; green - Caves et al., 2016). **B.** Reconstructed $p\text{CO}_2$ based on our measured $\delta^{11}\text{B}_{\text{carbonate}}$ values using different models for alkalinity and $\delta^{11}\text{B}_{\text{seawater}}$ from Greenop et al., 2017.

Figure 5: Reconstruction of surface $p\text{CO}_2$ for the past 0.8 My from *T. sacculifer* at ODP Sites 806 and 807. Also shown is benthic foraminiferal $\delta^{18}\text{O}$ with isotope stages labeled (black line – stack from Lisiecki and Raymo, 2005). $p\text{CO}_2$ values calculated from boron isotopes (colored symbols - this study) with data from the literature (gray symbols: circles - Hönisch et al., 2009; half filled circles - Seki et al. 2010; triangles – Foster et al., 2014; diamonds - Stap et al., 2016; squares – Chalk et al., 2017) and ice core $p\text{CO}_2$ (black line - LePetit et al., 2009). Data from the two sites we examined reproduces the absolute values and amplitude of atmospheric $p\text{CO}_2$ as determined from ice cores, thereby validating our methodology.

Figure 6: Proxy data for the past 17 million years in the Western Equatorial Pacific compared to benthic oxygen isotope data. **A.** Benthic $\delta^{18}\text{O}$ (blue line – stack from Lisiecki and Raymo, 2005; black line – compilation from Zachos et al., 2008). **B.** Benthic $\delta^{13}\text{C}$ (black line – compilation from Zachos et al., 2008). **C** to **E**, colored is indicating the site (open grey=806, filled grey=807), symbols represent the species (circle=*T. sacculifer* and triangle=*G. ruber*). **C.** SST reconstructed at ODP Sites 806 and 807 using Mg/Ca ratios and equation S6 and S7 (this study). **D.** Seawater pH reconstructed from $\delta^{11}\text{B}$ of *T. sacculifer* and *G. ruber* using $\delta^{11}\text{B}_{\text{seawater}}$ from Greenop et al. (2017) (refer to text and supplement for calculations, this study). **E.** Reconstructed $p\text{CO}_2$ (μatm) using boron-based pH and alkalinity from Caves et al. (2016), data presented are from this study. Propagated uncertainties are given by eq. S17 for the dark (green or blue) envelope, while the light (green or blue) envelope are the uncertainties calculated based on eq. S16 (taking into account uncertainty on $\delta^{11}\text{B}_{\text{seawater}}$).

Figure 7: Proxy data from 17 to 6 million years, including the Middle Miocene Climate Transition (MMCT) and Miocene Climate Optimum (MCO), in the Western Equatorial Pacific compared to benthic oxygen isotope data. **A.** Benthic $\delta^{18}\text{O}$ (black line – compilation from Zachos et al., 2008). **B.** Benthic $\delta^{13}\text{C}$ (black line – compilation from Zachos et al., 2008). **C** and **D**, colored is indicating the site (open grey=806, filled grey=807), symbols represent the species (circle=*T. sacculifer* and triangle=*G. ruber*). **C.** SST reconstructed at ODP Sites 806 and 807 using Mg/Ca ratios and equation



S6 and S7 (this study). **D.** Reconstructed pCO₂ (µatm) from this study (blue symbols) using boron-based pH and alkalinity from Caves et al. (2016). Propagated uncertainties are given by eq. S17 for the dark blue envelope, while the light blue envelope reflects the uncertainties calculated based on eq. S16 (taking into account uncertainty on δ¹¹B_{seawater}). In grey are δ¹¹B-derived estimates from the literature (open triangles – Foster et al., 2012 for Site 761B; half-filled diamonds – Foster et al., 2012 for Site 962A; open circles – Badger et al., 2013 for locality in Malta; half-filled triangles – Greenop et al., 2014 for Site 761B; filled diamonds – Stap et al., 2016 for Site 1264).

Figure 8: Proxy data from 7 to 1 million years, including the Warm Pliocene Transition (WPT), in the Western Equatorial Pacific compared to benthic oxygen isotope data. **A.** Benthic δ¹⁸O (black line – compilation from Zachos et al., 2008). **B.** Benthic δ¹³C (black line – compilation from Zachos et al., 2008). C and D, colored is indicating the site (open grey=806, filled grey=807), symbols represent the species (circle=*T. sacculifer* and triangle=*G. ruber*). **C.** SST reconstructed at ODP Sites 806 and 807 using Mg/Ca ratios and equation S6 and S7 (this study). **D.** Reconstructed pCO₂ (µatm) using boron-based pH and alkalinity from Caves et al. (2016), data presented are from this study. Propagated uncertainties are given by eq. S17 for the dark (green or blue) envelope, while the light (green or blue) envelope are the uncertainties calculated based on eq. S16 (taking into account uncertainty on δ¹¹B_{seawater}). In black are published estimates from ice core data (circles – Yan et al., 2019). In grey are δ¹¹B-derived estimates from the literature (light grey circles – Honisch et al., 2009 for Site 668B; half-filled circles – Seki et al., 2010 for Site 999A; medium grey circles – Bartoli et al., 2011 for Site 999A; unfilled triangles – Martinez-Boti et al., 2015b for Site 999A; squares – Chalk et al., 2017 for Site 999A; half-filled diamonds – Dyez et al., 2018 for Site 668B; grey triangles – de la Vega et al., 2020 for Site 999A).

Figure 9: Proxy data from 1.5 to 0.5 million years, including the Middle Pleistocene Transition (MPT), in the Western Equatorial Pacific compared to benthic oxygen isotope data. **A.** Benthic δ¹⁸O (blue line – stack from Lisiecki and Raymo, 2005). **B.** Benthic δ¹³C (black line – compilation from Zachos et al., 2008). C and D, colored is indicating the site (open grey=806, filled grey=807), symbols represent the species (circle=*T. sacculifer* and triangle=*G. ruber*). **C.** SST reconstructed at ODP Sites 806 and 807 using Mg/Ca ratios and equations S6 and S7 (this study). **D.** Reconstructed pCO₂ (µatm) using boron-based pH and alkalinity from Caves et al. (2016), data presented are from this study. Propagated uncertainties are given by eq. S17 for the dark (green or blue) envelope, while the light (green or blue) envelope are the uncertainties calculated based on eq. S16 (taking into account uncertainty on δ¹¹B_{seawater}). In black are published estimates from ice core data (line – LePetit et al., 2009; circles – Yan et al., 2019). In grey are δ¹¹B-derived estimates from the literature (grey circles – Honisch et al., 2009 for Site 668B; half-filled circles – Seki et al., 2010 for Site 999A; squares – Chalk et al., 2017 for Site 999A; half-filled diamonds – Dyez et al., 2018 for Site 668B).

Figure 10: Proxy data from 1.5 to 0.5 million years, including the Middle Pleistocene Transition (MPT), in the Western Equatorial Pacific compared to benthic oxygen isotope composites. **A.** Benthic δ¹⁸O (blue line – compilation from Lisiecki and Raymo, 2005, black line – compilation from Zachos et al. 2008). **B.** Records from Lithium isotopes (δ⁷Li, orange, Misra and Froelich, 2012) and Strontium isotopes (^{87/86}Sr, grey, Hodell et al., 1991, Farrel et al., 1995, Martin et al., 1999, Martin et al., 2004), both proxies for silicate weathering. Orange arrows represent the different weathering regimes as indicated by the δ⁷Li, black crosses are indication when changes in weathering regime occurs. **C.** Reconstructed pCO₂ (µatm) using boron-based pH and alkalinity from Caves et al. (2016), data presented are from this study (circle – *T. sacculifer* and triangle – *G. ruber*). Propagated uncertainties are given by eq. S17 for the dark (green or blue) envelope, while the light (green or blue) envelope are the uncertainties calculated based on eq. S16 (taking into account uncertainty on δ¹¹B_{seawater}). In grey are δ¹¹B-derived estimates from the literature (light grey circles – Honisch et al., 2009 for Site 668B; half-filled circles – Seki et al., 2010 for Site 999A; medium grey circles – Bartoli et al., 2011 for Site 999A; unfilled triangles – Foster et al., 2012 for Site 761B; top half-filled diamonds – Foster et al. 2012 for Site 962A; open squares – Badger et al., 2013 for locality in Malta;



left-filled triangle – Greenop et al., 2014 for Site 761B; upside down triangle – Foster et al., 2014 for Site 999A; grey triangles – Martinez-Boti et al., 2015b for Site 999A; grey diamonds – Stap et al., 2016 for Site 1264; grey squares – Chalk et al., 2017 for Site 999A; bottom half-filled diamonds – Dyez et al., 2018 for Site 668B; grey triangles - de la Vega et al., 2020 for Site 999A). Also shown are timing of major events. The rose band and dark rose band indicate eruption of the Columbia River flood basalts (Hooper et al., 2002) and time of maximum eruption (Kasbohm and Schoene, 2018), respectively. Light grey bands represent hypothesized La Nina-like intervals and dashed dark grey bands represent hypothesized El Nino-like intervals (Farell et al., 1995; Chaisson and Ravelo, 2000; Nathan and Leckie, 2009; Ford et al., 2012; Drury et al., 2018). The biogenic bloom in the EEP (Farell et al., 1995) and in the WEP (Berger et al., 1991) is hypothesized to have been driven by enhanced weathering that increased nutrient delivery to the global ocean (Hermoyian and Owen, 2001).



Table 1: Boxe core information.

Cruise	Leg	Hole	N (°)	E (°)	Depth (m)
ODP	130	807	3.61	156.62	3638
ODP	130	806	0.32	159.37	2521



Table 2: Comparison of reconstructed pCO₂ values for key intervals in the last 17 Myr.

Mid-Pleistocene transition (1.2-0.8 Ma)						
MIS (G)	pCO ₂ (µatm)	Reference	MIS (IG)	pCO ₂ (µatm)	Reference	pCO ₂ amplitude IG-G (µatm)
20	171	This study	21	245	This study	74
22	180	This study	23	222	This study	42
24	<i>nd</i>		25	288	This study	<i>nd</i>
26	168	This study	27	<i>nd</i>		<i>nd</i>
28	165	This study	29	<i>nd</i>		<i>nd</i>
30	164	This study	31	295	Hönisch et al., 2009 (N-TIMS)	131
32	218	Chalk et al., 2017	33	323	Chalk et al., 2017	105
34	197	Chalk et al., 2017	35	315	Chalk et al., 2017	118
36	189	Chalk et al., 2017	37	295	This study, Chalk et al., 2017	106
			39	306	This study	<i>nd</i>
Early Pliocene Warm Period (4.7-4.5 Ma)						
pCO ₂ (µatm)	Reference					
541 ± 124	This study (2 SD, n=3)					
Middle Pliocene Warm Period (3.29-2.97 Ma)						
pCO ₂ (µatm)	Reference					
515 ± 119	This study (2 SD, n=4)					
320 ± 130	Martinez-Boti, 2015b (2 SD, n=8)					
Miocene Climate Optimum (17-14 Ma)						
pCO ₂ (µatm)	Reference					
479 ± 173	This study (2 SD, n=4)					
350-400	Foster et al., 2012					
300-500	Greenop et al., 2014					
470-630	Sosdian et al., 2018					

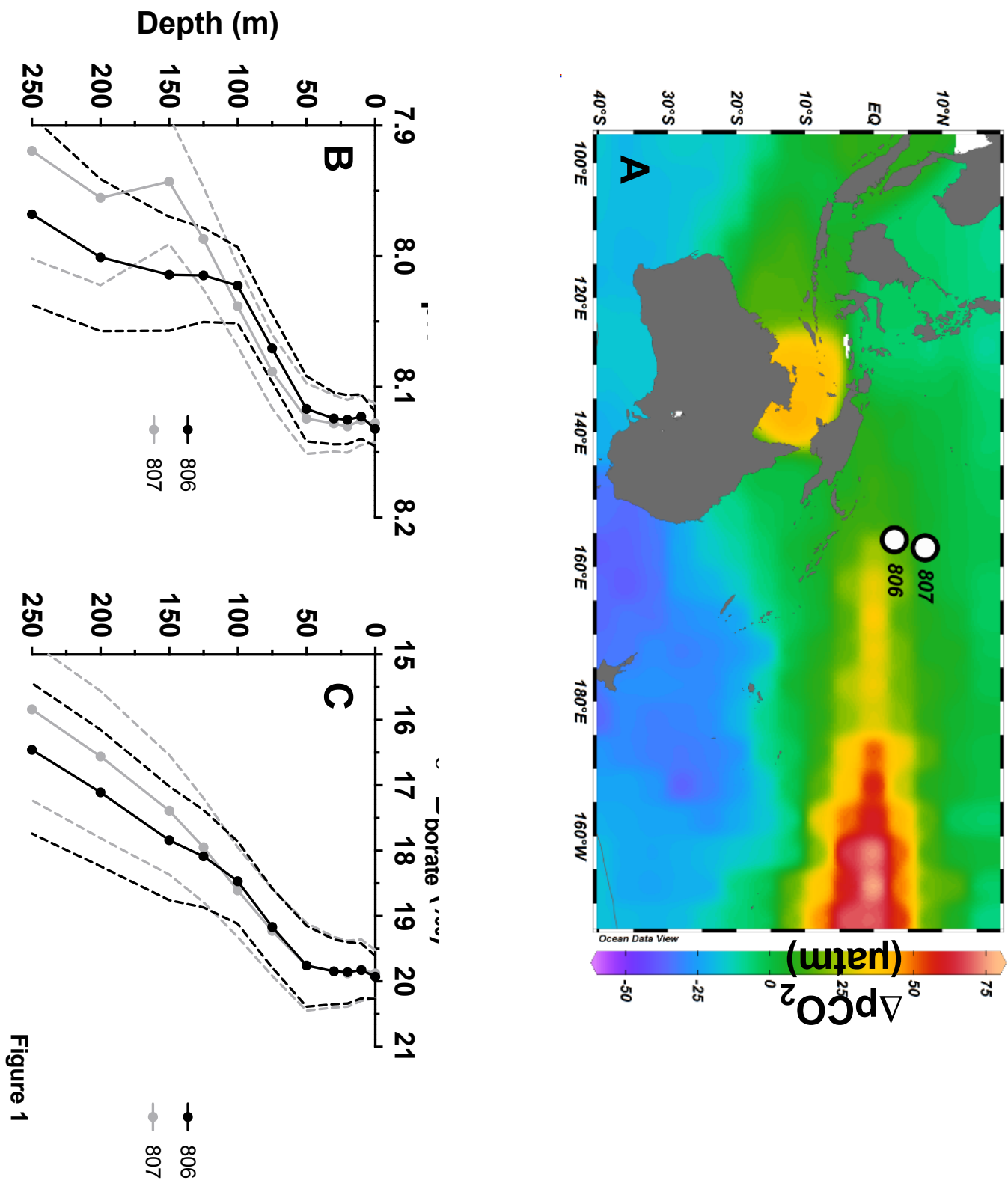


Figure 1 31

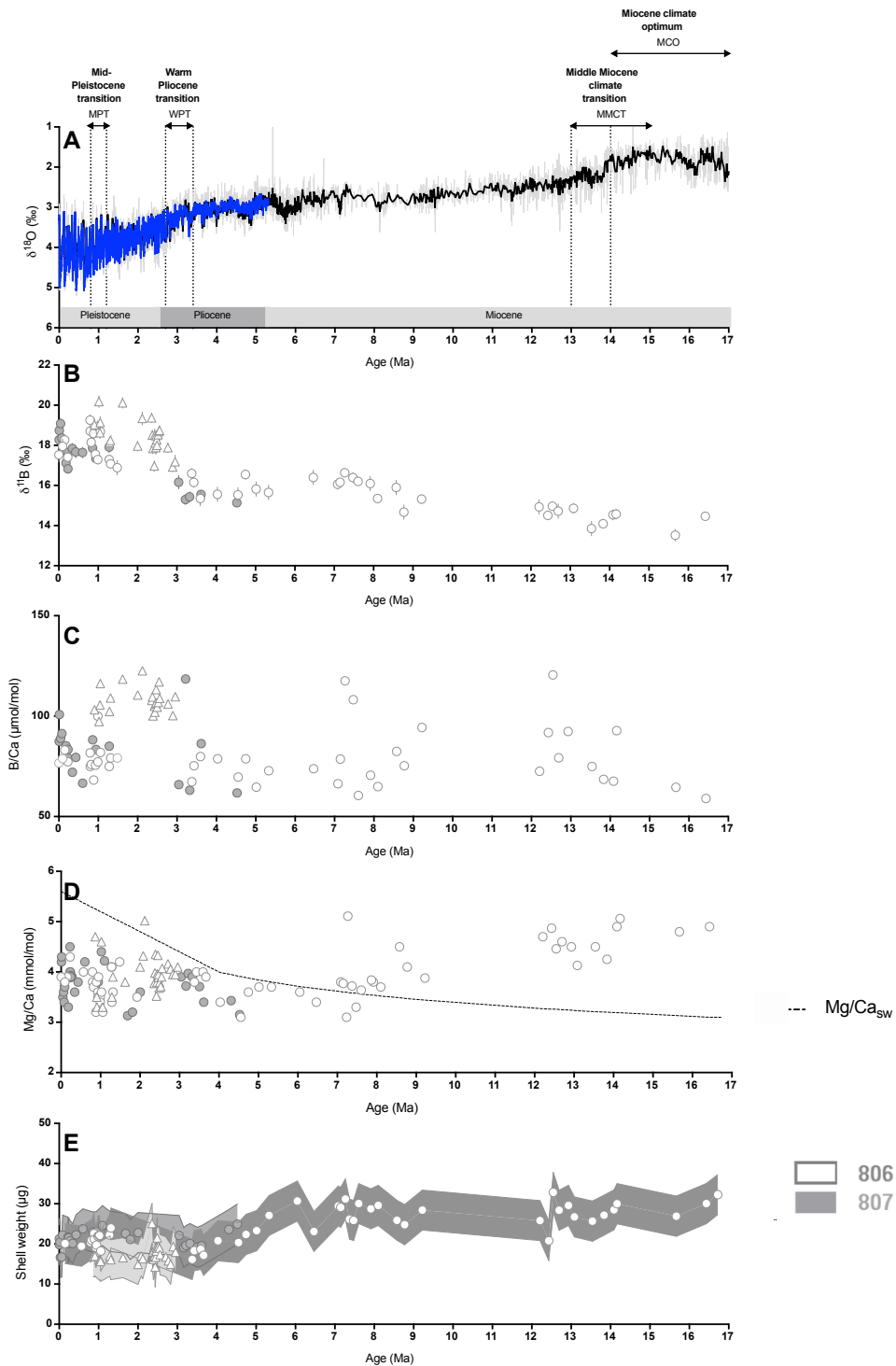


Figure 2

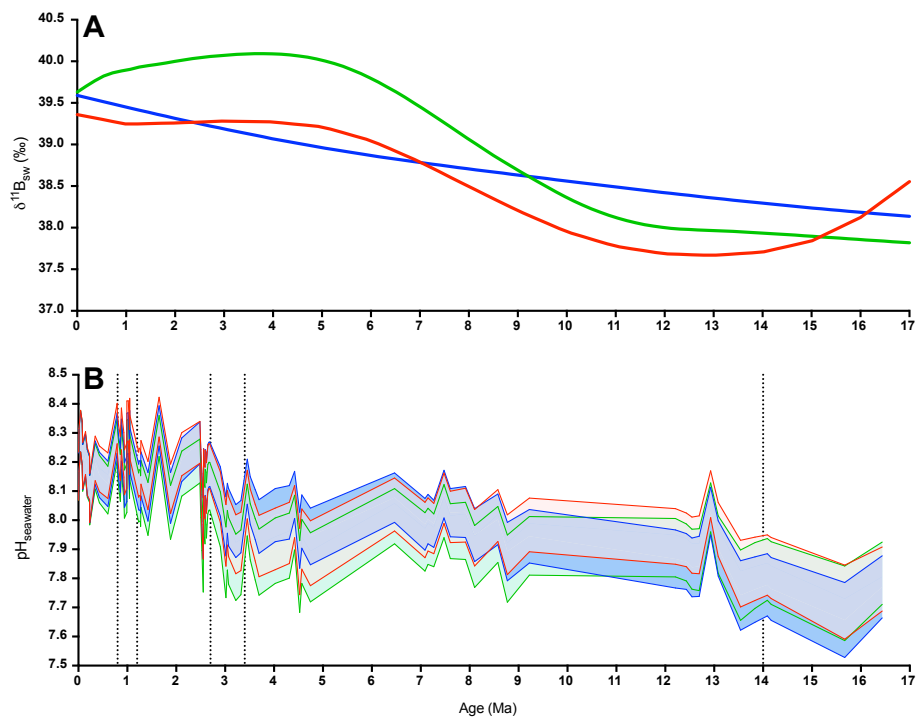


Figure 3

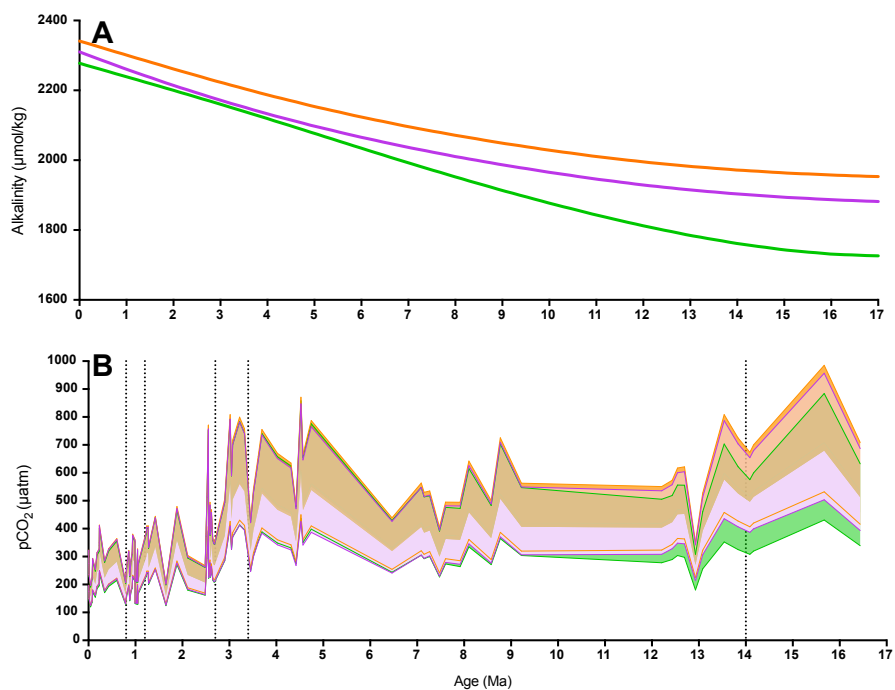


Figure 4

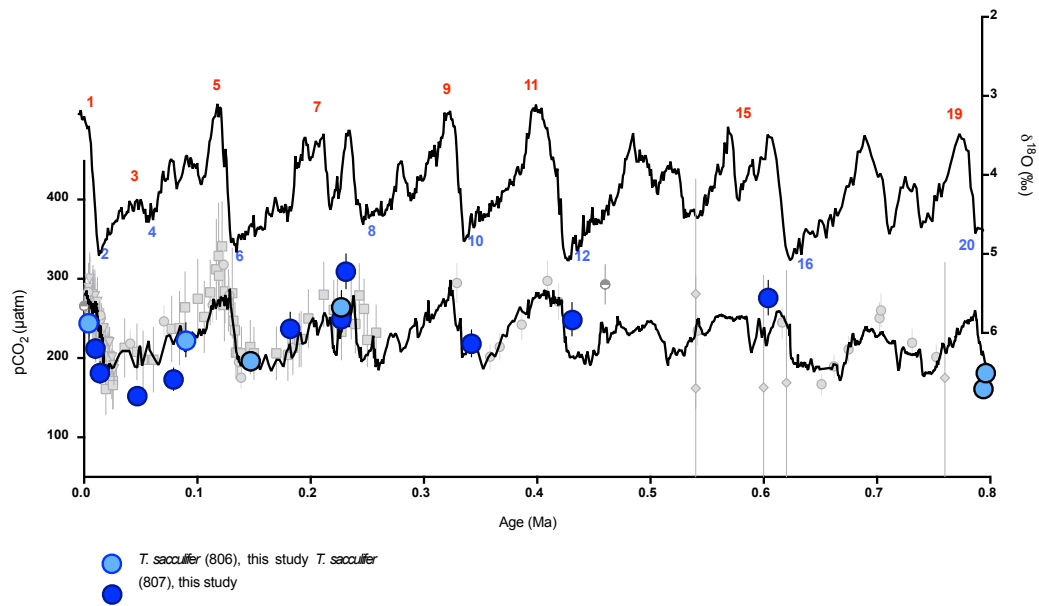


Figure 5

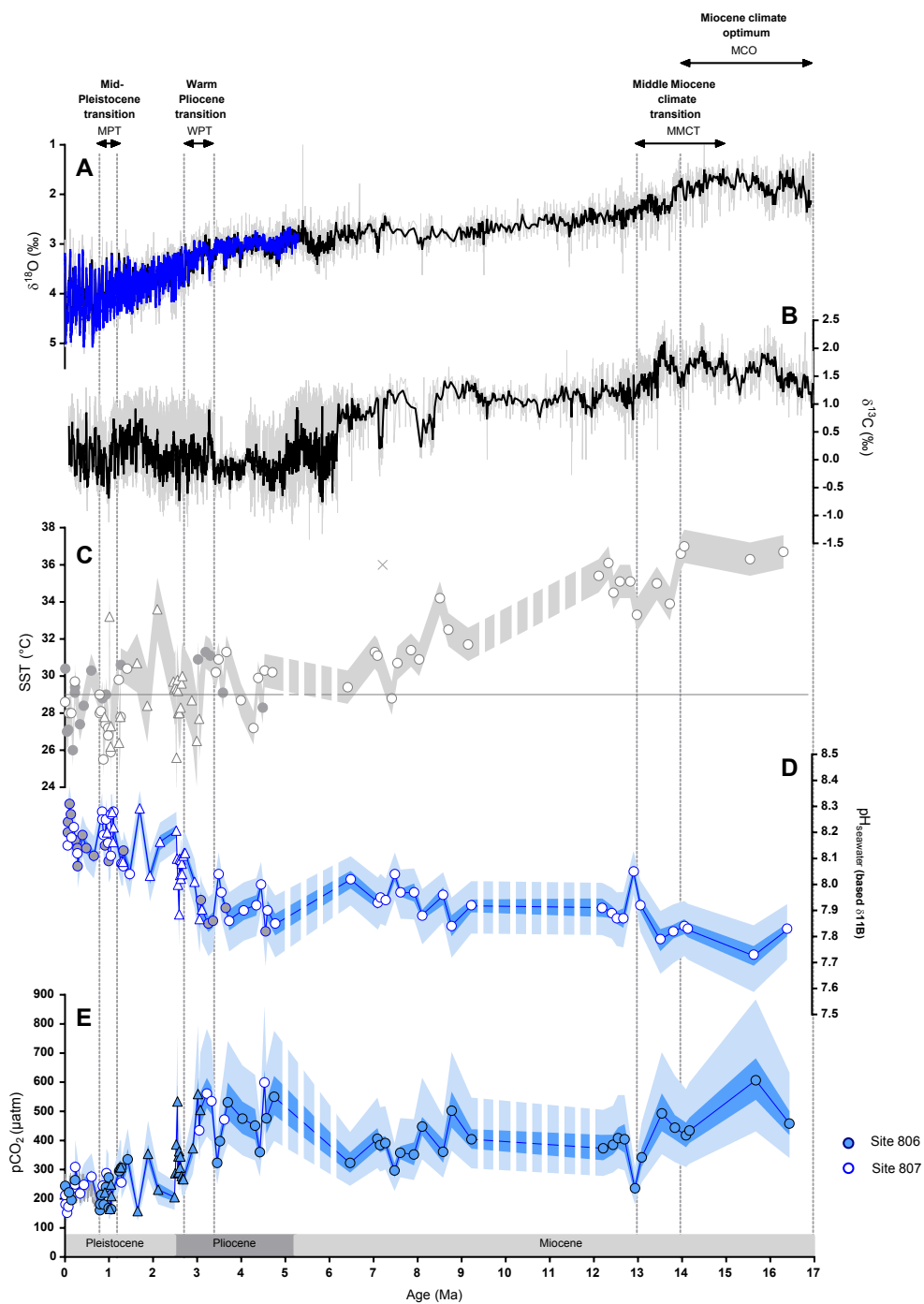


Figure 6

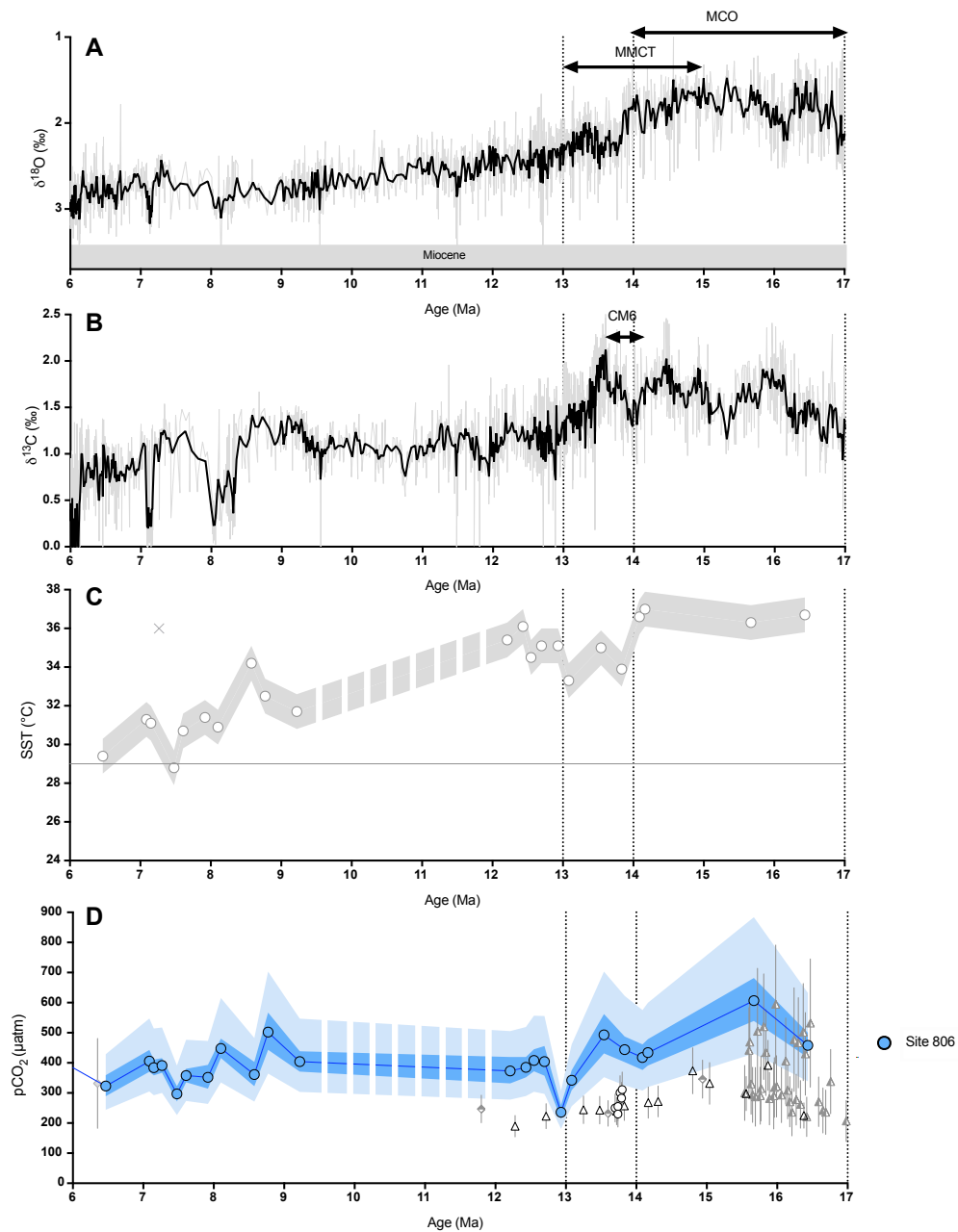


Figure 7

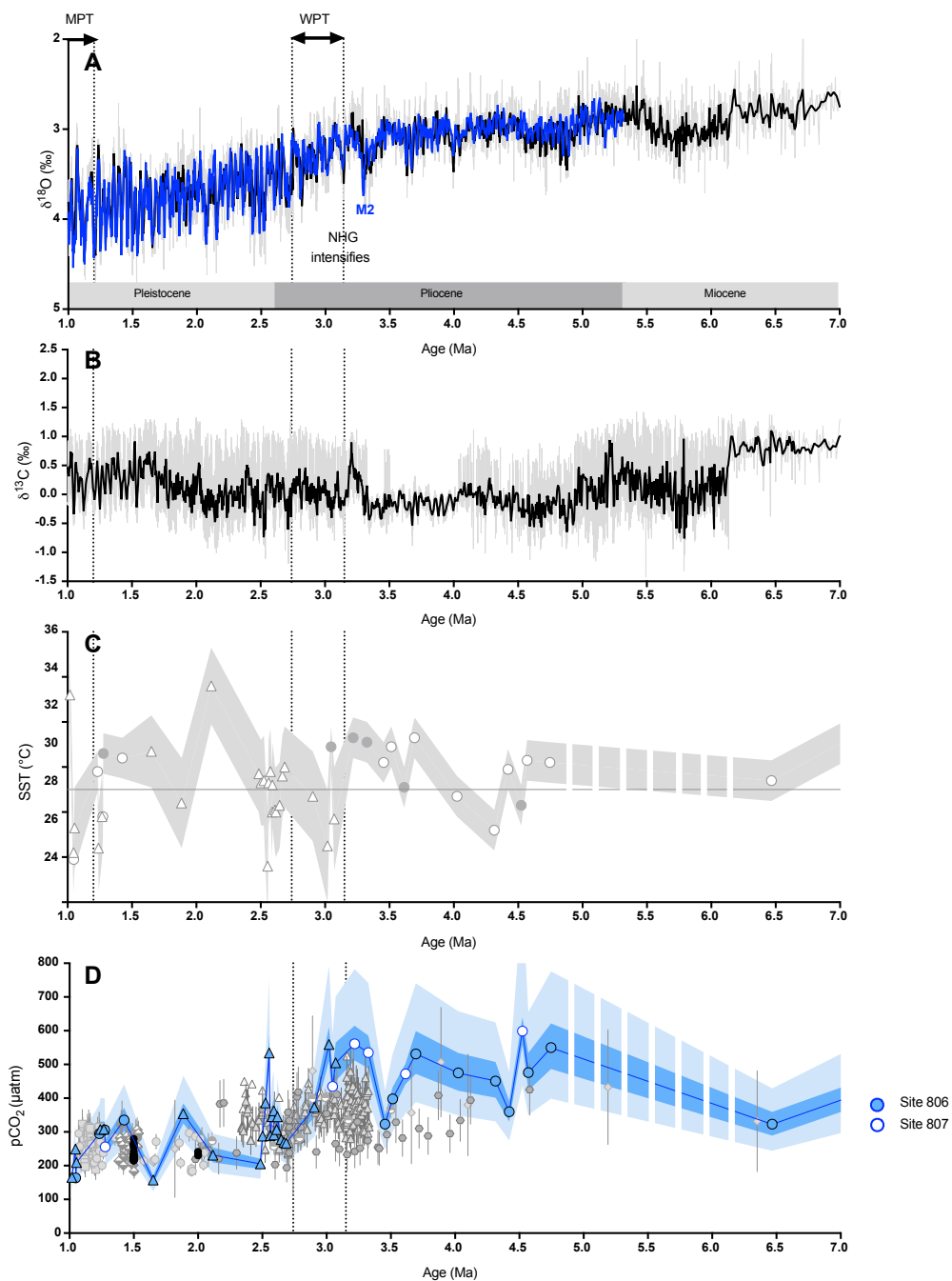


Figure 8

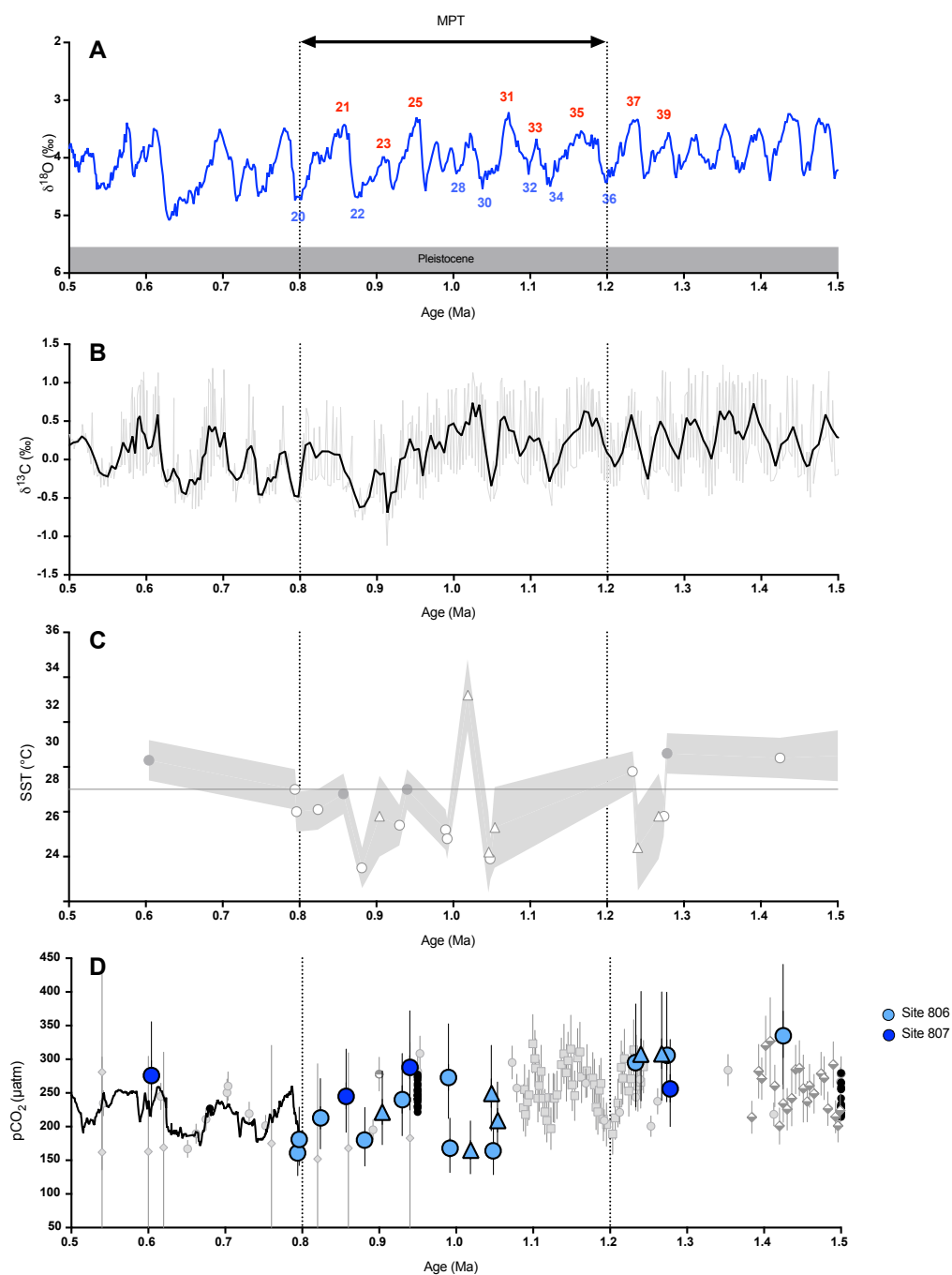


Figure 9

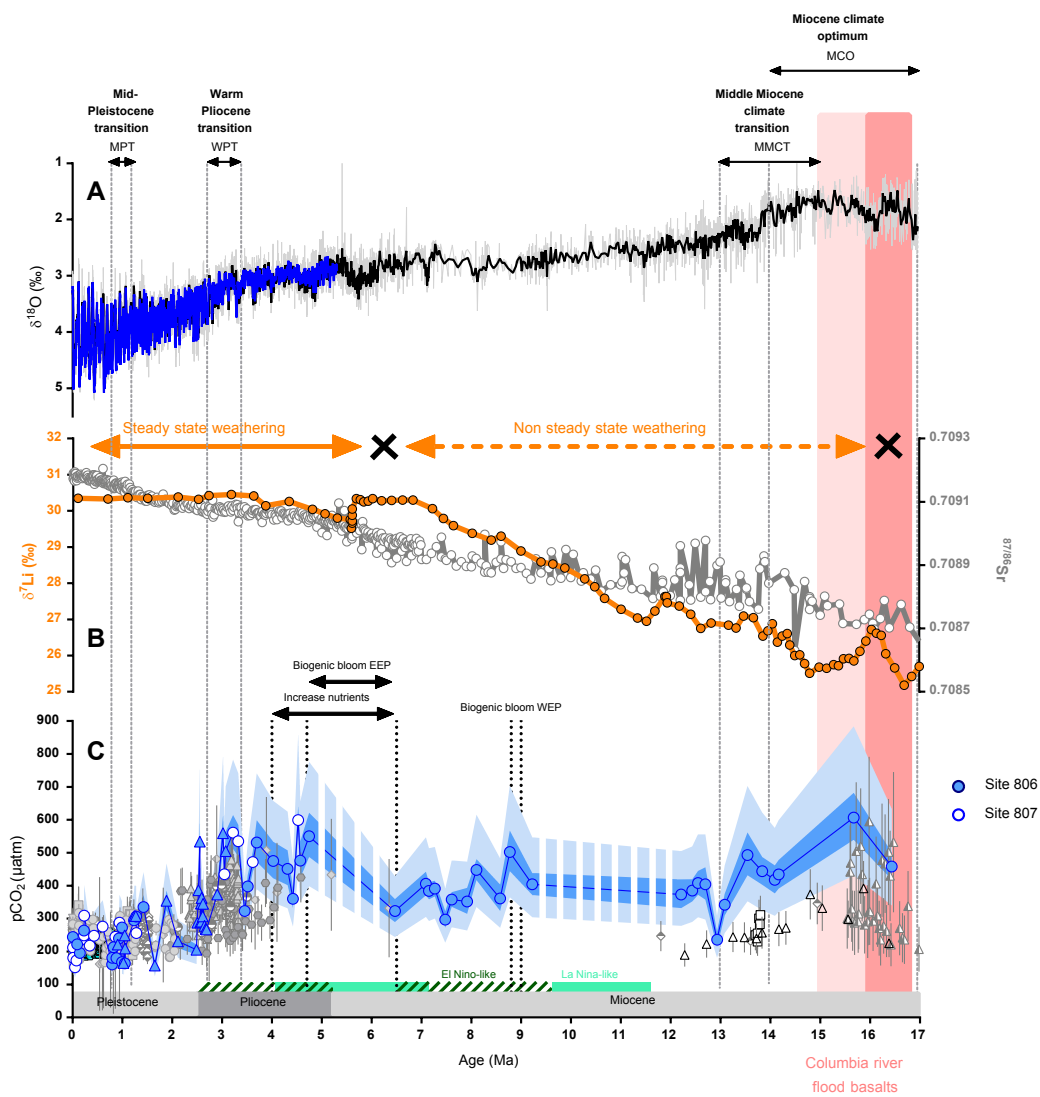


Figure 10